Beamforming Design in Reconfigurable Intelligent Surface-Assisted IoT Networks Based on Discrete Phase Shifters and Imperfect CSI

Sajjad Nassirpour, *Graduate Student Member, IEEE*, Alireza Vahid, *Senior Member, IEEE*,
Dinh-Thuan Do, *Senior Member, IEEE*, and Dinesh Bharadia, *Member, IEEE*

Abstract—In this article, we study reconfigurable intelligent surface (RIS)-assisted networks to support Internet of Things (IoT) devices. We propose RIS beamforming strategies to maximize sum rate and fairness and analyze the RIS location. We derive a theoretical lower bound of the minimum number of RIS elements needed to guarantee specific network performance metrics and validate our results via simulations. We present two RIS scenarios in this study, both with the same total number of RIS elements: 1) centralized RIS, where a single RIS assists the network and 2) distributed RIS, where each transmitter has its own dedicated RIS. We study addressing two practical challenges related to RIS elements and channel state information (CSI) assumptions. First, we consider hardware limitations by assuming that each RIS element is equipped with a discrete phase shifter (PS). Second, we investigate the impact of CSI perfectness and availability in the network; therefore, we evaluate the performance of the RIS-assisted network under two scenarios: 1) centralized RIS with imperfect global CSI and 2) distributed RIS, where imperfect local CSI is available at each transmitter.

Index Terms—Beamforming, channel state information (CSI), distributed transmitters, fading channels, integer programming, Internet of Things (IoT), reconfigurable intelligent surface (RIS), throughput.

I. INTRODUCTION

IN THE past few years, Internet of Things (IoT) communication networks have enabled devices with sensing, processing, and communication capabilities to provide a wide range of services, such as intelligent manufacturing, emergency detection, and structural health monitoring with minimal human interaction [1]. To fully utilize the potential of IoT networks, two research challenges need to be addressed.

1) The issue of massive connectivity is foreseen as hundreds of billions of IoT devices will be in operation by 2030 [2], and this results in a co-channel interference issue.
2) Many IoT devices rely on batteries, which are supposed to last for ten years or more, and this necessitates to development of power-efficient solutions [3].

To address these challenges, one solution is to allocate a unique chunk of spectrum to each IoT device, which is not a scalable solution due to the scarcity of the spectrum. Furthermore, massive multiple-input multiple-output (MIMO) with a large number of antennas is an attractive beamforming technique to support IoT devices, which creates a focused beam for the desired IoT device while simultaneously providing nulls at undesired devices. Nevertheless, this approach is power hungry as each antenna is connected to a single radio frequency (RF) chain, thereby increasing the complexity and cost of the method.

A promising application of programmable metasurfaces called reconfigurable-intelligent-surface (RIS) has been recently introduced. An RIS comprises a large number of passive elements, specifically phase shifters (PSs), that are intelligently tuned to substantially improve wireless communication performance. On the one hand, RIS has the capability to enhance signal quality, making it possible to accommodate IoT devices in scenarios with massive connectivity. Moreover, RIS offers low-cost hardware with low-power consumption due to its passive reflectors. As a result, RIS could be a solution to respond to the aforementioned challenges and therefore has found a vast number of applications in IoT networks, including but not limited to joint beamforming, to enhance over-the-air computation [4], improving secrecy rate [5], and unmanned aerial vehicle (UAV) communications [6].

A. State-of-the-Art

The exceptional features of RIS have garnered significant attention from both academia and industry, leading to apply RIS-based beamforming techniques to enhance the performance of wireless communication networks, such as maximizing the sum rate and improving fairness among the IoT devices [7], [8], [9]. In particular, Zheng et al. [7] studied an RIS-assisted multiuser multiple-input single-output (MISO) wireless-powered communication network, where the users

harvest energy in the downlink and transmit their information simultaneously in the uplink to a single access point (AP). Zheng et al. [7] maximized the weighted sum rate by jointly optimizing the active beamforming at the AP and the passive beamforming at RIS. Next, Xie et al. [9] investigated an RIS-assisted multicell MISO network to suppress the intercell interference. They focused on a max-min fairness problem and applied an alternative optimization (AO) method to jointly optimize the AP beamforming and the RIS elements.

As we mentioned earlier, IoT networks confront a massive connectivity challenge. Consequently, assuming distributed APs in the network supporting multiple IoT devices is a more realistic scenario. Motivated by this, Fu et al. [10] considered an RIS-assisted MIMO device-to-device network with distributed APs and then maximized the achievable degrees of freedom (DoF) by jointly designing the PSs at RIS and transceiver coding matrices. However, the extent to which RIS beamforming and active beamforming at the transceivers contribute to the overall benefit is unclear. Therefore, in the first part of this work, similar to [11], we focus on pure RIS gain by considering a single-input single-output (SISO) network with distributed APs that uses a single RIS, which we refer to as a centralized RIS, to support multiple IoT devices. Here, we design RIS beamforming to maximize sum rate and optimize fairness.

Previous studies have typically considered Rayleigh fading for channels without a Line of Sight (LoS), Rician fading for channels with an LoS link, and Nakagami fading for scenarios involving multipath where one path is non-LoS but stronger [7], [8], [9], [10], [12]. In our work, we comprehensively evaluate the performance of our RIS-assisted network under Rayleigh, Rician, and Nakagami fading models.

The construction of a PS with infinite-bit resolution is difficult due to manufacturing issues [13]. Thus, discrete PSs are utilized in real-world scenarios, which turn the optimization problem into a nonconvex nonlinear integer programming (NLIP) problem that is NP-hard. To the best of our knowledge, a brute-force search is the only method to obtain the global optimum solution of an NLIP problem, which examines all possible solutions. However, the brute-force search is not a practical approach due to its extremely high complexity. Thus, Gong et al. [14] and Abdullah et al. [15] proposed a successive-refinement (SR) algorithm to optimize the discrete PSs at RIS. However, this approach only provides local optimal solutions. In this article, we introduce a low-complexity optimization method based on filled function, which directly targets discrete PSs to optimize the RIS elements and uses filled function to move from one local optimum solution to a better one.

Apart from optimizing the RIS elements, it is important to determine the RIS location. Placing the RIS close to either the transmitter or receiver is a possible solution to mitigate the impact of product-path loss in the Tx-RIS-Rx link, but it may not always be practical due to user mobility or physical constraints. To address this issue, networks utilizing multiple RISs, referred to as the distributed RIS scenario, have been proposed to improve the performance of the RIS-assisted networks [16], [17], [18], [19], [20]. Specifically, a strategy based on double-RISs was proposed in [16], where one RIS is located near the AP, and the other is placed near a cluster of users. However, assuming one RIS near the users can be challenging. Next, Do et al. [17] studied the statistical characterization and modeling of a network with distributed RISs, while the results were limited to a point-to-point scenario, and RIS elements were not optimized. Then, Yang et al. [18] focused on a distributed RIS-MIMO-non orthogonal multiple access (NOMA) system and used discrete PSs as the RIS elements, Galappaththige et al. [19] proposed a distributed RIS scenario in a cell-free massive MIMO setup to maximize the sum rate, and Mei and Zhang [20] applied a beamforming technique in a MIMO network assisted by distributed RIS to optimize fairness among the users.

As RIS uses passive elements, it requires many elements to enhance the network performance, and this increases the number of channels significantly. Yang et al. [18], Galappaththige et al. [19], and Mei and Zhang [20] assumed that AP obtains perfect global channel state information (CSI) prior to communications through the pilot signals. However, in real-world scenarios, the channel estimation process faces two main challenges.

1) *Imperfect CSI:* It is feasible to have an error in the estimation process due to hardware impairments, noise, and so on, which results in imperfect CSI, and hence affects the beamforming strategies at AP and RIS [21].

2) *CSI Availability:* A large number of channels in the RIS-assisted network, especially with multiple RISs, necessitates a large bandwidth for the feedback signals from the IoT devices to the AP, and this could be a bottleneck in the network.

As a result, in the second part of this article, we investigate a network with distributed RISs, where one RIS is dedicated to each AP. In this case, we assume each AP knows its outgoing imperfect channels to all IoT devices, and beyond that, it only knows the statistics of the other channels. We define this as local CSI at transmitter (CSIT).

Moreover, we analytically derive a lower bound of the minimum number of RIS elements needed to achieve a desired performance metric (e.g., per-user rate) and analyze the results as a function of the location of the RIS.

Table I represents the main differences between our work and the literature.

B. Our Main Contributions

We provide more details about our contributions below.

1) We consider SISO RIS-assisted IoT networks with distributed transmitters. We study RIS beamforming to maximize the sum rate and address the max-min optimization problems. We evaluate the performance of our network using relevant channel models. In particular, we first analyze the results under Rayleigh fading analytically and numerically. Then, we focus on numerical evaluation for Rician and Nakagami fading models.

2) We focus on discrete PSs, which result in nonconvex NLIP optimization problems. We propose a heuristic method based on the filled function to solve the problem.

TABLE I
MAIN DIFFERENCES BETWEEN OUR WORK AND THE LITERATURE

	Our paper	[7]	[9]	[12]	[10]	[11]	[16]	[14]	[15]	[21]	[18]	[19]	[20]
Multiple RISs	✓						✓				✓	✓	✓
Sum-rate maximization	✓	✓			✓				✓			✓	
Max-min rate optimization	✓		✓				✓	✓					✓
Rayleigh fading	✓	✓								✓			✓
Rician fading	✓		✓		✓		✓	✓	✓				
Nakagami fading	✓			✓							✓	✓	
Distributed transmitters	✓				✓	✓						✓	
Pure RIS gain	✓					✓						✓	
Low-bit phase shifters	✓							✓	✓		✓		
Imperfect CSI	✓									✓			
Local CSIT	✓												
Lower-bound on the number of RIS elements	✓												

We compare the efficiency of our approach with two SR-based methods as well as a genetic algorithm (GA) and a simplified exhaustive search (SES) method in terms of complexity and rate.

3) We study the RIS placement in our work, and quantify the minimum number of RIS elements required to achieve specific network objectives, such as sum rate or fairness, and we validate the results through simulations, which would provide valuable practical guidelines.

4) We delve into the practical considerations related to CSI perfectness and availability in RIS-assisted networks. Specifically, we examine two RIS scenarios: a) centralized RIS, where a single RIS assists the network to serve multiple IoT devices simultaneously, and imperfect CSI is available globally and b) distributed RIS, where each AP has its own dedicated RIS, and each AP knows its local CSIT. Notice that both scenarios utilize the same total number of RIS elements to serve IoT devices. Our simulation findings indicate that the latter scenario not only achieves a higher sum rate than the former but also requires fewer RIS elements to attain a given sum rate.

The remainder of this article is organized as follows. We present our channel model and outline the optimization problem in Section II. In Section III, we discuss our proposed optimization approach. Then, in Section IV, we provide a lower bound on the minimum number of required RIS elements. Section V presents the simulation results, and Section VI concludes this article.

C. Notations

Throughout this article, we use bold-face lowercase, bold-face uppercase, and italic letters to denote vectors, matrices, and scalars, respectively. We also use $\mathbb{C}^{I \times J}$ to describe the space of $I \times J$ complex-valued matrices. diag$\{\mathbf{x}\}$ is a diagonal matrix using vector $\mathbf{x}$, and $|\mathbf{x}|$ and $||\mathbf{x}||$ are the absolute value and Euclidean norm of complex-valued vector $\mathbf{x}$, respectively. We use $\mathbb{E}(\cdot)$, $\log(\cdot)$, $Re(\cdot)$, and $Im(\cdot)$ to denote the statistical expectation, logarithmic function in base 2, and real and imaginary parts of a complex number, respectively. Finally, $\mathbf{B}^{H}$ shows the conjugate transpose of matrix $\mathbf{B}$.

II. PROBLEM SETTING

This article focuses on an RIS-assisted IoT network with K single-antenna distributed APs (transmitters) and K single-antenna IoT devices (receivers). We consider two RIS-based scenarios: 1) centralized RIS, suitable when the RIS can be positioned near the transmitters or receivers and 2) distributed RIS, where each transmitter is equipped with a dedicated RIS. Fig. 1 shows the network model, which could capture the communication dynamics of real-world IoT networks with massive connectivity, such as smart cities and Industrial IoT (IIoT) networks, where RIS(s) can be installed on building facades or factory walls, respectively.

A. Centralized RIS

In this case, we use a centralized RIS with M reconfigurable elements as shown in Fig. 1(a), where Tx_i, RIS, and Rx_i are available at $(x_t^{[i]}, y_t^{[i]})$, (x_0, y_0), and $(x_r^{[i]}, y_r^{[i]})$, $i = 1, 2, \ldots, K$, respectively.

Channel Model: We use $h_d^{[ji]}(t) \in \mathbb{C}^{1 \times 1}$, $\mathbf{h}^{[j]}(t) \in \mathbb{C}^{M \times 1}$, and $\mathbf{g}^{[i]}(t) \in \mathbb{C}^{1 \times M}$ to denote the channels of Tx_j-Rx_i link (between Tx_j and Rx_i, $i, j \in \{1, 2, \ldots, K\}$), Tx_j-RIS link, and RIS-Rx_i link, respectively, at time t. We assume RIS elements are spaced at least $\lambda/2$ apart from each other where λ is the wavelength of the transmitted signal. Thus, the elements of $\mathbf{h}^{[j]}(t)$ and $\mathbf{g}^{[i]}(t)$ are independent across time and users.

CSI Perfectness: We assume each receiver estimates its incoming channels from all transmitters perfectly and then informs the others about these channels through two cases.

1) The noiseless links, which represent that other network nodes learn the channels perfectly as the receiver (noiseless CSI).

2) The noisy links, meaning that the information provided to the transmitters is noisy and thus imperfect. We refer to this as "noisy-p" channels if other nodes attain the imperfect channels at a signal-to-noise ratio (SNR) of p dB.

CSI Availability: Similar to [7], [8], [9], [10], and [11], we assume global CSI is accessible throughout the network, and there is no further data exchange between the transmitters. Additionally, no data is exchanged beyond CSI between the receivers.

Small-Scale Fading: Similar to [22], [23], and [24], since in practice, RIS is usually positioned with the knowledge of the AP's location, we consider $\mathbf{h}^{[j]}(t)$ is an LoS channel vector (i.e., $\mathbf{h}^{[j]}(t) = \mathbf{h}^{[j]}$). On the contrary, due to the user's mobility and the complex propagation environment, assuming $h_d^{[ji]}(t)$ and $\mathbf{g}^{[i]}(t)$ are LoS channels is impossible in practice; thus,
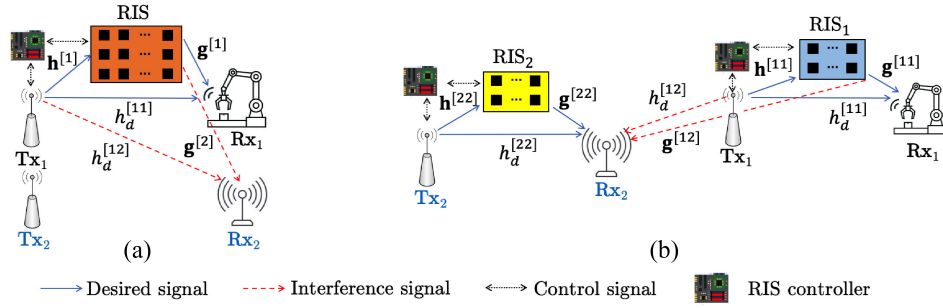
Fig. 1. SISO IoT networks with distributed transmitters and (a) centralized RIS and (b) distributed RISs.

we assume $h_d^{[ji]}(t)$ and $\mathbf{g}^{[i]}(t)$ are distributed based on Rayleigh fading. Here, we write $h_m^{[j]}$, the mth element of $\mathbf{h}^{[j]}$, as follows:

$$h_m^{[j]} = e^{-j\frac{2\pi}{\lambda} d_{\mathsf{Tx}_j - \mathrm{RIS}[m]}} \tag{1}$$

where $d_{\mathsf{Tx}_j - \mathrm{RIS}[m]}$ shows the distance between Tx_j and the mth element of the RIS. In addition, $h_d^{[ji]}(t)$ and $g_m^{[i]}(t)$ (the mth element of $\mathbf{g}^{[i]}(t)$) are distributed based on $\mathcal{CN}(0, \sigma_{h_d}^2)$ and $\mathcal{CN}(0, \sigma_g^2)$, respectively, where $\sigma_{h_d}^2$ and σ_g^2 show the corresponding variances. Later, in Section V, we will evaluate the performance of our RIS-assisted network by considering Rician and Nakagami fading models as more realistic channel fading models.

Large-Scale Fading: We use $C_0 d^{-\alpha}$ as the path loss profile where C_0 describes the signal loss at a reference distance (e.g., 1 m), d is the distance between a pair of nodes (e.g., Tx_j and Rx_i), and α represents the corresponding path loss exponent.

For simplicity, in the rest of this article, we use m_h, $\sigma_{h_d}^2$, and σ_g^2 to denote $h_m^{[j]}$, the variance of $h_d^{[ji]}(t)$, and the variance of each element of $\mathbf{g}^{[i]}(t)$, respectively, which include the impact of both small-scale fading and large-scale fading. In this work, we assume that the array aperture of RIS is relatively small, leading to a correspondingly small Rayleigh distance. As a consequence, the channels primarily fall within the far-field region, and the influence of the near-field is deemed negligible.

RIS Configuration: We assume a controller between Tx_1 and RIS to exchange CSI and control the RIS elements over a separate link. Moreover, we consider only the first reflected signal from the RIS due to the significant path loss; thus, if $\tilde{x}(t)$ is the incident signal at time t, we find the reflected signal from the mth element of the RIS as

$$\tilde{y}_m(t) = \tilde{x}(t)\left(\beta_m(t)e^{j\theta_m(t)}\right), \quad 1 \le m \le M \tag{2}$$

where $\beta_m(t) \in [0, 1]$ and $\theta_m(t) \in [0, 2\pi)$ are the amplitude and phase of the mth element of the RIS, respectively, at time t. For simplicity, we consider $\beta_m(t) = 1$ in this work. We also assume that each RIS element has a b-bit PS, indicating that each RIS element can only take $N = 2^b$ quantized levels. We define ϕ_N, the set of quantized values of $\theta_m(t)$, as

$$\phi_N = \left\{0, \frac{2\pi}{N}, \frac{4\pi}{N}, \dots, \frac{2\pi(N-1)}{N}\right\}. \tag{3}$$

Moreover, we use $\Theta(t) \in \mathbb{C}^{M \times M}$ to denote the RIS configuration, which is given by

$$\Theta(t) = \mathrm{diag}\left\{e^{\boldsymbol{\theta}(t)}\right\}, \quad \boldsymbol{\theta}(t) = [\theta_1(t), \theta_2(t), \dots, \theta_M(t)]. \tag{4}$$

Received Signal: The received signal at Rx_i is a combination of the direct signals from the APs and the reflected signals from the RIS, which is given by

$$y_i(t) = \sum_{j=1}^{K}\left[\mathbf{g}^{[i]}(t)\Theta(t)\mathbf{h}^{[j]} + h_d^{[ji]}(t)\right]x_j(t) + n_i(t) \tag{5}$$

where $x_j(t)$ is the transmitted signal at Tx_j, $n_i(t) \sim \mathcal{CN}(0, \sigma^2)$ is additive white Gaussian noise (AWGN) at Rx_i, and $\mathbb{E}\{\mathbf{x}(t)\mathbf{x}^H(t)\} = \mathrm{diag}([P_1, P_2, \dots, P_K])$ where $\mathbf{x}(t) = [x_1(t), x_2(t), \dots, x_K(t)] \in \mathbb{C}^{1 \times K}$ and $P_j, j \in \{1, 2, \dots K\}$ describes the transmit power from Tx_j. As we describe later, all operations occur in a single coherence time; therefore, the time notation is removed throughout the rest of this work. In this work, we assume that the coherence time, and thus the coherence distance, is large enough so that all evaluations involve communication channels experiencing flat fading during each time slot. Then, we use (5) and write the signal-to-interference-plus-noise ratio (SINR) at Rx_i as follows:

$$\mathrm{SINR}_i = \frac{P_i\left|\mathbf{g}^{[i]}\Theta\mathbf{h}^{[i]} + h_d^{[ii]}\right|^2}{\sigma^2 + \sum_{j=1, j \ne i}^{K} P_j\left|\mathbf{g}^{[i]}\Theta\mathbf{h}^{[j]} + h_d^{[ji]}\right|^2}. \tag{6}$$

B. Distributed RIS

As depicted in Fig. 1(b), we have K distributed RISs, one dedicated RIS to each transmitter, where each RIS has (M/K)[1] elements (i.e., total RIS elements is equal to M). We assume the same location notations for the transmitters and the receivers as discussed in Section II-A and use $(x_0^{[i]}, y_0^{[i]})$ to denote the location of RIS$_i$, the ith RIS.

Channel Model: We use $\mathbf{h}^{[ji]} \in \mathbb{C}^{M \times 1}$, and $\mathbf{g}^{[ii]} \in \mathbb{C}^{1 \times M}$ to denote the channels of Tx_j-RIS$_i$, $i, j = 1, 2, \dots, K$ and RIS$_i$-Rx_i links, respectively. Notice that $h_d^{[ji]}$, large-scale fading, and small-scale fading are similar to the case with a centralized RIS. However, since RIS$_i$ is dedicated to Tx_i, assuming LoS channels between Tx_j and RIS$_i$ is not feasible. As a result,

---

[1]Without loss of generality, we assume M is divisible by K.

we assume that $\mathbf{h}^{[ji]}$ is distributed based on Rayleigh fading whose elements have $\mathcal{CN}(0, \tilde{\sigma}_h^2)$ distribution.

CSI Perfectness: Here, we assume two channel knowledge cases as noiseless and noisy-p channels.

CSI Availability: Acquiring global CSI requires an excessive overhead because of the substantial number of channels in the RIS-assisted network. This overhead would create a bottleneck in practice as feedback channels have limited bandwidth [25], [26], [27], [28], [29], [30] and the delay overhead may render forward communications infeasible [31], [32]. Therefore, in distributed RIS case, we consider no data exchange between the transmitters and focus on a more realistic assumption as Tx$_i$ is aware of its outgoing channels to the receivers (the direct channels and the channels through RIS$_i$) and beyond that, it only knows the statistics of the other channels. We refer to this model as local CSIT [25], [27], [28]. Further, Rx$_i$ knows its incoming channels from all transmitters plus the outgoing channels from Tx$_i$ to compute the optimal configuration at RIS$_i$ and beyond that, it only knows the statistics of the other channels. There is no data exchange beyond CSI between the receivers.

RIS Configuration: We assume Tx$_i$ uses a controller to exchange CSI and control the PSs at RIS$_i$ via a separate link. Similar to the centralized case, we consider only the first reflected signal from each RIS and use $\theta_m^{[i]} \in \phi_N$ to denote the phase shift at the mth element of RIS$_i$. Then, we use $\Theta^{[i]} \in \mathbb{C}^{M \times M}$ to show the RIS configuration at RIS$_i$ as

$$\Theta^{[i]} = \mathrm{diag}\left\{e^{\boldsymbol{\theta}^{[i]}}\right\}, \quad \boldsymbol{\theta}^{[i]} = \left[\theta_1^{[i]}, \theta_2^{[i]}, \ldots, \theta_M^{[i]}\right]. \quad (7)$$

Received Signal: According to the channel coefficients and $\Theta^{[i]}$, we find the received signal at Rx$_i$, which is given by

$$y_i = \left[\sum_{i'=1}^{K} \mathbf{g}^{[i'i]}\Theta^{[i']}\mathbf{h}^{[ii']} + h_d^{[ii]}\right]x_i \quad (8)$$
$$+ \sum_{j=1, j \neq i}^{K}\left[\sum_{i'=1}^{K} \mathbf{g}^{[i'i]}\Theta^{[i']}\mathbf{h}^{[ji']} + h_d^{[ji]}\right]x_j + n_i.$$

Notice that the assumptions about x_i, transmit power P_i, and n_i are similar to the assumptions described in (5). Based on (8), we compute the SINR at the ith receiver as follows:

$$\mathrm{SINR}_i = \frac{P_i\left|\sum_{i'=1}^{K} \mathbf{g}^{[i'i]}\Theta^{[i']}\mathbf{h}^{[ii']} + h_d^{[ii]}\right|^2}{\sigma^2 + \sum_{j=1, j \neq i}^{K} P_j\left|\sum_{i'=1}^{K} \mathbf{g}^{[i'i]}\Theta^{[i']}\mathbf{h}^{[ji']} + h_d^{[ji]}\right|^2}. \quad (9)$$

C. Optimization Problem

One of our goals in this work is to find the RIS configuration that maximizes the sum rate. Therefore, we define the following optimization problem with a centralized RIS

$$\max_{\boldsymbol{\theta}} \underbrace{\sum_{i=1}^{K} \log(1 + \mathrm{SINR}_i)}_{\triangleq -q(\boldsymbol{\theta})} \equiv \min_{\boldsymbol{\theta}} q(\boldsymbol{\theta})$$
$$\text{s.t. } \boldsymbol{\theta} = [\theta_1, \theta_2, \ldots, \theta_M], \ \theta_m \in \phi_N, \ 1 \leq m \leq M. \quad (10)$$

Moreover, to meet fairness among users, we define a max-min optimization problem as

$$\max_{\boldsymbol{\theta}} \min_{i=\{1,2,\ldots,K\}} \log(1 + \mathrm{SINR}_i)$$
$$\text{s.t. } \boldsymbol{\theta} = [\theta_1, \theta_2, \ldots, \theta_M], \ \theta_m \in \phi_N, \ 1 \leq m \leq M. \quad (11)$$

Notice that (10) and (11) are NLIP problems, and as we discussed in Section I, there is no efficient way to find the global optimum solution for them. Hence, an NLIP problem can be solved through two methods.

1) Converting it to an equivalent convex approximation problem and then applying a regular convex optimizer, such as CVX [33], to find the approximated solution. Li et al. [8] converted (10) into a format known as the difference of convex (DC) problem and then applied the successive convex approximation (SCA) method, an iterative approach, to find an equivalent convex form of the DC problem. Additionally, Zheng et al. [16] focused on (11) and employed semidefinite relaxation (SDR) and bisection methods to discover a quasi-convex equivalent for (11). Nevertheless, Li et al. [8] and Zheng et al. [16] made certain approximations in their approach, potentially compromising the optimality of their solutions;

2) Using a heuristic method (e.g., SR, filled function, and GA), which directly focuses on the original problem. This allows for solving both (10) and (11) using a single optimizer.

Gong et al. [14] and Abdullah et al. [15] utilized the SR-based methods, which are iterative algorithms that optimize each of the RIS elements alternately while fixing the other $M-1$ elements in an iterative manner until convergence is achieved. However, these methods tend to converge to local solutions. Therefore, in this article, we focus on heuristic methods and propose an optimization method based on sigmoid filled function to optimize (10) and (11). In the next section, we show how our approach moves from one local optimum solution to a better one using the filled function.

Since only local CSIT is available to each transmitter in the distributed case, it is not feasible to maximize the sum rate. Thus, in Section III-B, we will define *score$_i$* in (17) for Tx$_i$ and formulate the optimization problem accordingly.

III. PROPOSED OPTIMIZATION APPROACH

A. Centralized RIS

The idea of the filled function optimization method was originally introduced in [34] for the continuous domain. Then, Ng et al. [35] updated it for the discrete domain. In this article, we use a sigmoid-based filled function and run local and global searches to optimize (10).

Local Search: We define $\mathcal{N}(\boldsymbol{\theta})$ as the neighbors of RIS configuration $\boldsymbol{\theta}$ such that

$$\mathcal{N}(\boldsymbol{\theta}) = \boldsymbol{\theta} \cup \{\boldsymbol{\theta} + \boldsymbol{\lambda}_m, \boldsymbol{\lambda}_m \in \boldsymbol{\Lambda}\} \quad (12)$$

where $\boldsymbol{\lambda}_m$ is an M-length column vector with the mth element chosen from $\{0, (2\pi/N), (4\pi/N), \ldots, ([2\pi(N-1)]/N)\}$ and the others set to zero; further, $\boldsymbol{\Lambda}$ is the direction set equals

---

Algorithm 1 Local Search

Input: $\boldsymbol{\theta}_\ell$, $i_{\max}^{\text{loc}}$;
Output: $\boldsymbol{\theta}^*$;
1: $i_\ell^{\text{loc}} = 0$; $\boldsymbol{\theta}^* = \boldsymbol{\theta}_\ell$;
2: **for** $\lambda_m \in \Lambda$ **do**
3: $\quad \tilde{\boldsymbol{\theta}} = \boldsymbol{\theta}_\ell + \lambda_m$;
4: $\quad$ **if** $q(\tilde{\boldsymbol{\theta}}) < q(\boldsymbol{\theta}^*)$ **then**
5: $\quad\quad \boldsymbol{\theta}^* = \tilde{\boldsymbol{\theta}}$;
6: $i_\ell^{\text{loc}} \leftarrow i_\ell^{\text{loc}} + 1$;
7: **if** $\boldsymbol{\theta}^* \neq \boldsymbol{\theta}_\ell$ and $i_\ell^{\text{loc}} \leq i_{\max}^{\text{loc}}$
$\quad$ **then**
8: $\quad \boldsymbol{\theta}_\ell = \boldsymbol{\theta}^*$;
9: $\quad$ Go to line 2;
10: **else**
11: $\quad \boldsymbol{\theta}^*$ is the local mini-
$\quad$ mizer.

Algorithm 2 Global Search

Input: $\boldsymbol{\theta}_0$, r, τ, ϵ, $i_{\max}^{\text{loc}}$, $i_{\max}^{\text{filled}}$;
Output: $\boldsymbol{\theta}^{**}$;
1: $\ell = 0$; $r_0 = r$; $\bar{\tau} = \tau$;
2: $i_m^{\text{filled}} = 0$, for $m = 0, 1, \ldots, (N-1)M$;
3: $\boldsymbol{\theta}^{**} = \boldsymbol{\theta}_0$;
4: **if** $\ell + 1 \geq \bar{\tau}$ **then**
5: $\quad \bar{\tau} \leftarrow \bar{\tau} + \tau$;
6: $\quad$ Run Algo. 1 with $\boldsymbol{\theta}_\ell$
$\quad$ and (10) to find $\boldsymbol{\theta}_\ell^*$;
7: **else**
8: $\quad \boldsymbol{\theta}_\ell^* = \boldsymbol{\theta}_\ell$;
9: **if** $q(\boldsymbol{\theta}_\ell^*) < q(\boldsymbol{\theta}^{**})$ or $\ell = 0$ **then**
10: $\quad \boldsymbol{\theta}^{**} = \boldsymbol{\theta}_\ell^*$; $r = r_0$;
11: $\quad m = 1$;
12: $\quad$ Run Algo. 1 with $\boldsymbol{\theta}_\ell^*$
$\quad$ and (13) to get $\bar{\boldsymbol{\theta}}_\ell^*$;
13: $\quad i_{m-1}^{\text{filled}} \leftarrow i_{m-1}^{\text{filled}} + 1$
14: **if** $m = 1$ **then**
15: $\quad \ell \leftarrow \ell + 1$;
16: $\quad \boldsymbol{\theta}_\ell = \bar{\boldsymbol{\theta}}_{\ell-1}^*$;
17: **else**
18: $\quad \boldsymbol{\theta}_\ell = \bar{\boldsymbol{\theta}}_\ell^*$;
19: Go to line 4;
20: **if** $m \leq (N-1)M$ **then**
21: $\quad \boldsymbol{\theta}_\ell^* = \boldsymbol{\theta}_{\ell-1}^* + \lambda_m$;
22: $\quad m \leftarrow m + 1$;
23: $\quad$ Go to line 12;
24: **else**
25: $\quad$ **if** $\sum_{m=0}^{(N-1)M} i_m^{\text{filled}} > i_{\max}^{\text{filled}}$ or $r < \epsilon$ **then**
26: $\quad\quad \boldsymbol{\theta}^{**}$ is selected as
$\quad\quad$ global minimizer.
27: $\quad$ **else**
28: $\quad\quad r \leftarrow \frac{r}{10}$;
29: $\quad\quad \ell \leftarrow \ell - 1$;
30: $\quad\quad$ Go to line 11;

---

to $\Lambda = \{\lambda_m, m = 1, 2, \ldots, M\}$. Here, the local search scans all neighbors of $\boldsymbol{\theta}$ to find a solution as $\boldsymbol{\theta}^* \in \mathcal{N}(\boldsymbol{\theta})$ such that $q(\boldsymbol{\theta}^*) < q(\boldsymbol{\theta})$. If we cannot find such $\boldsymbol{\theta}^*$, we call $\boldsymbol{\theta}^* = \boldsymbol{\theta}$ the local minimizer; otherwise, we consider $\boldsymbol{\theta} = \boldsymbol{\theta}^*$ and repeat the local search.

We provide Algorithm 1 to demonstrate how the local search works. We use i_ℓ^{loc} to denote the number of iterations to find the local optimizer in the ℓth round of using Algorithm 1. Then, we define $i_{\max}^{\text{loc}}$ as the maximum value of i_ℓ^{loc}. Initially, we set $i_\ell^{\text{loc}} = 0$ and $\boldsymbol{\theta}^* = \boldsymbol{\theta}_\ell$, and then, in lines 2 to 5, we check all the neighbors around $\boldsymbol{\theta}_\ell$ to find a better solution than $\boldsymbol{\theta}_\ell$. To do this, we set $\tilde{\boldsymbol{\theta}} = \boldsymbol{\theta}_\ell + \lambda_m$. If $q(\tilde{\boldsymbol{\theta}}) < q(\boldsymbol{\theta}^*)$, $\tilde{\boldsymbol{\theta}}$ offers a better solution than $\boldsymbol{\theta}^*$; hence, we set $\boldsymbol{\theta}^* = \tilde{\boldsymbol{\theta}}$. Following the completion of the search among $\boldsymbol{\theta}_\ell$'s neighbors, we increase i_ℓ^{loc} by one. If $\boldsymbol{\theta}^* = \boldsymbol{\theta}_\ell$ or $i_\ell^{\text{loc}} > i_{\max}^{\text{loc}}$, we consider $\boldsymbol{\theta}^*$ to be the local minimizer. Otherwise, we use $\boldsymbol{\theta}_\ell = \boldsymbol{\theta}^*$ and repeat lines 2 to 5 for all neighbors of new $\boldsymbol{\theta}_\ell$.

Global Search: The filled function plays an essential role in the global search. In this work, we use filled function $Q_r(\boldsymbol{\theta}, \boldsymbol{\theta}^*)$ and define an auxiliary optimization problem as

$$\min_{\boldsymbol{\theta}} Q_r(\boldsymbol{\theta}, \boldsymbol{\theta}^*)$$
$$\text{s.t.} \quad \boldsymbol{\theta}, \boldsymbol{\theta}^* \in \phi_N \tag{13}$$

where $\boldsymbol{\theta}^*$ is the current local minimizer of (10), and $r > 0$ denotes the filled function parameter. The aim here is to find a better solution than $\boldsymbol{\theta}^*$. The global search begins with random configuration $\boldsymbol{\theta}_0$ and uses the local search for (10) to obtain $\boldsymbol{\theta}_0^*$ as its local minimizer. Then, to find a better solution, it exploits a sigmoid filled function, which is given by

$$Q_r(\boldsymbol{\theta}, \boldsymbol{\theta}^*) = \left(1 + \frac{1}{1 + \beta||\boldsymbol{\theta} - \boldsymbol{\theta}^*||^2}\right) f_r(q(\boldsymbol{\theta}) - q(\boldsymbol{\theta}^*)) \tag{14}$$

where

$$f_r(q(\boldsymbol{\theta}) - q(\boldsymbol{\theta}^*))$$
$$= \begin{cases} q(\boldsymbol{\theta}) - q(\boldsymbol{\theta}^*) + r, & q(\boldsymbol{\theta}) - q(\boldsymbol{\theta}^*) \leq -r \\ \frac{1}{1 + e^{\frac{-6}{r}(q(\boldsymbol{\theta}) - q(\boldsymbol{\theta}^*) + r/2)}}, & -r < q(\boldsymbol{\theta}) - q(\boldsymbol{\theta}^*) < 0 \\ 1, & q(\boldsymbol{\theta}) - q(\boldsymbol{\theta}^*) \geq 0 \end{cases} \tag{15}$$

and

$$\beta = \begin{cases} 0, & q(\boldsymbol{\theta}) - q(\boldsymbol{\theta}^*) \leq -r \\ 1, & \text{otherwise.} \end{cases} \tag{16}$$

It applies $\boldsymbol{\theta}_0^*$ to (14) and runs the local search for (13) to obtain $\tilde{\boldsymbol{\theta}}_0^*$. Next, it assumes $\boldsymbol{\theta}_1 = \tilde{\boldsymbol{\theta}}_0^*$ and runs the local search for (10)

with $\boldsymbol{\theta}_1$ to attain $\boldsymbol{\theta}_1^*$ as a new local minimizer. We call $\boldsymbol{\theta}_1^*$ a better solution than the previous local minimizer if $q(\boldsymbol{\theta}_1^*) < q(\boldsymbol{\theta}_0^*)$. It repeats this procedure until a stopping criterion is satisfied. Here, we use r as the optimization parameter. Intuitively, r denotes a radius around $\boldsymbol{\theta}^*$ that the algorithm seeks for a new solution. If the global search fails to identify a better solution with r, it reduces r by using $r = r/10$, resulting in a smaller search area surrounding the local minimizer. Notice that if the global search discovers a new solution, it resets r to its initial value. Moreover, we use $i_m^{\text{filled}}, m = 0, 1, 2, \ldots, (N-1)M$ to denote the number of times our method searches for a new solution by scanning the mth neighbor of a local minimizer obtained from (13). Then, we define $i_{\max}^{\text{filled}}$ as the maximum number of times the global search uses the filled function to search for a new solution. Finally, we stop the procedure if $\sum_{m=0}^{(N-1)M} i_m^{\text{filled}} > i_{\max}^{\text{filled}}$ or $r < \epsilon$, for some $\epsilon \ll 1$ (e.g., $\epsilon = 0.01$), and declare the latest solution as the output of the global search.

Then, to accelerate the search process, in this article, we modify the global search and use the local search to optimize (10) every $\tau \in \mathbb{N}$ times. More precisely, after τ times of finding the local minimizer of the auxiliary optimization problem, we run the local search for (10) to minimize $q(\boldsymbol{\theta})$.

We provide Algorithm 2 to describe the global search. The algorithm's inputs are $\boldsymbol{\theta}_0$, $r > 1$, $\tau \geq 1$, $\epsilon \ll 1$, $i_{\max}^{\text{loc}}$, and $i_{\max}^{\text{filled}}$, where $\boldsymbol{\theta}_0$ is selected randomly. Here, the output is $\boldsymbol{\theta}^{**}$, and we use ℓ, r_0, and $\bar{\tau}$ to denote the ℓth round of the global search, to keep the initial value of r, and to show which round of the global search uses the local search for (10), respectively. Initially, we set $\ell = 0$, $r_0 = r$, $\bar{\tau} = \tau$, $i_m^{\text{filled}} = 0, m = 0, 1, \ldots, (N-1)M$, and $\boldsymbol{\theta}^{**} = \boldsymbol{\theta}_0$. Then, if $\ell + 1 \geq \bar{\tau}$, we update $\bar{\tau}$ and run the local search for (10) with $\boldsymbol{\theta}_\ell$ to get its local minimizer as $\boldsymbol{\theta}_\ell^*$. Otherwise, we skip the local search and consider $\boldsymbol{\theta}_\ell^* = \boldsymbol{\theta}_\ell$. Next, if $q(\boldsymbol{\theta}_\ell^*) < q(\boldsymbol{\theta}^{**})$ or $\ell = 0$, we set

θ_ℓ^* as a new optimal solution, reset the value of r ($r = r_0$), and put $m = 1$ where m represents the index of a neighbor around θ_ℓ^*. Then, we use the local search for (13) with θ_ℓ^* to obtain $\bar{\theta}_\ell^*$ and set $i_{m-1}^{\text{filled}} \leftarrow i_{m-1}^{\text{filled}} + 1$. If $m = 1$, we increase ℓ by one and set $\theta_\ell = \bar{\theta}_{\ell-1}^*$; else, the algorithm knows that it searched at least one of the neighbors around θ_ℓ^* and put $\theta_\ell = \bar{\theta}_\ell^*$. Then, it goes to line 4. Thereafter, if $q(\theta_\ell) \geq q(\theta^{**})$, the global search checks whether it covers all the neighbors around θ_ℓ^* or not. If the answer is no, it updates θ_ℓ^*, increases m by one, and goes to line 12. Otherwise, if $\sum_{m=0}^{(N-1)M} i_m^{\text{filled}} > i_{\text{max}}^{\text{filled}}$ or $r < \epsilon$, it stops the searching process and declares θ^{**} as the global minimizer; else, it confines the searching area by reducing r. Then, it sets $\ell \leftarrow \ell - 1$ and goes to line 11.

Remark 1: We note that the filled function-based optimization methods can optimize a general nonlinear objective function as long as selecting a possible configuration from a discrete set is the only constraint. This model is usually referred to as an unconstrained optimization problem [35].

According to Remark 1, we can apply our sigmoid filled function method to the max-min optimization problem in (11).

B. Distributed RIS

In this case, we assume each transmitter only knows its own local CSIT; therefore, we define $score_i$ as a new objective function that captures the fact of enhancing the desired signals from Tx_i, $i = 1, 2, \ldots, K$ at Rx_i while suppressing the interference signals from Tx_i at other receivers. Consequently, we write $score_i$ as

$$score_i \triangleq \frac{P_i \left| \mathbf{g}^{[ii]} \Theta^{[i]} \mathbf{h}^{[ii]} + h_d^{[ii]} \right|^2}{\sigma^2 + \sum_{j=1, j \neq i}^{K} P_i \left| \mathbf{g}^{[ij]} \Theta^{[i]} \mathbf{h}^{[ii]} + h_d^{[ij]} \right|^2} \quad (17)$$

where compared to SINR_i given in (6), the denominator includes noise and the interference caused by Tx_i at unintended receivers. Then, we define the optimization problem for RIS_i, $1 \leq i \leq K$, as follows:

$$\max_{\theta^{[i]}} score_i$$
$$\text{s.t. } \theta^{[i]} = \left[\theta_1^{[i]}, \theta_2^{[i]}, \ldots, \theta_M^{[i]} \right], \ \theta_m^{[i]} \in \phi_N, \ 1 \leq m \leq M. \quad (18)$$

Here, we use the same strategy as Section III-A to maximize (18) since the filled function can be applied to a general unconstrained optimization problem.

IV. MINIMUM NUMBER OF REQUIRED RIS ELEMENTS

Prior results, for the most part, either do not consider the number of RIS elements and instead focus on adjusting the elements of a given RIS [36] or obtain the number of RIS elements at high SNRs [11]. On the contrary, in this work, we compute a lower bound on the minimum number of RIS elements to guarantee to achieve a specific value of SINR at each receiver.

A. Centralized RIS

Usually, RIS elements are configured based on channel coefficients; however, to find a lower bound on M in this work, we assume that θ is independent of the channels and selected randomly with uniform distribution. This assumption has been used in [37] and [38] for switch-based beamforming techniques. For simplicity, we focus on a symmetric scenario, which includes the following.

1) All transmitters have the same transmit power (i.e., $P_i = P$, $i \in \{1, 2, \ldots K\}$).
2) Each receiver stands at the same distance from all transmitters.
3) The distance between the RIS and all transmitters are the same.
4) The receivers are placed at the same distance from the RIS.

We use the following two lemmas to explain our analysis.

Lemma 1 [37]: If $\mathbf{g}^{[i]}$ shows the channel vector between RIS and Rx_i, whose elements are independent and identically distributed (i.i.d.) random variables with zero mean and variance σ_g^2, and $\mathbf{h}^{[j]}$ denotes the LoS channel vector between Tx_j and RIS with value m_h. Then, for a given RIS configuration Θ, where all elements are drawn independently at random from $\{0, (2\pi/N), \ldots, ([2\pi(N-1)]/N)\}$, the variance of $\mathbf{g}^{[i]} \Theta \mathbf{h}^{[j]}$ is equal to

$$\nu = M \sigma_g^2 (m_h)^2. \quad (19)$$

Proof: We have

$$\nu = \text{var}\left(\sum_{m=1}^{M} g_m^{[i]} e^{j\theta_m} h_m^{[j]} \right) \overset{(a)}{=} \sum_{m=1}^{M} \text{var}\left(g_m^{[i]} e^{j\theta_m} \right) (m_h)^2$$
$$\overset{(b)}{=} \sum_{m=1}^{M} \left(\sigma_g^2 \underbrace{\text{var}\left(e^{j\theta_m} \right)}_{1} + \sigma_g^2 \underbrace{\left[\mathbb{E}\left(e^{j\theta_m} \right) \right]^2}_{=0} \right) (m_h)^2$$
$$+ \sum_{m=1}^{M} \underbrace{\left[\mathbb{E}\left(g_m^{[i]} \right) \right]^2}_{=0} \text{var}\left(e^{j\theta_m} \right) (m_h)^2 = M \sigma_g^2 (m_h)^2 \quad (20)$$

where $\text{var}(X)$ denotes the variance of X. Here, (a) holds since $h_m^{[j]}$ is constant and $e^{j\theta_m}$ and $g_m^{[i]}$ are independent. Further, (b) follows the rule of the variance of the product of two independent variables. Hence, (20) completes the proof. ∎

Lemma 2: For any $\delta_{ji} > 0$, $i, j \in \{1, 2, \ldots, K\}, j \neq i$

$$\Pr\left(\left| \mathbf{g}^{[i]} \Theta \mathbf{h}^{[j]} \right| < \frac{\delta_{ji}}{2} \Big| \Theta \right) > \Pr\left(\left| Re\{ \mathbf{g}^{[i]} \Theta \mathbf{h}^{[j]} \} \right| < \frac{\delta_{ji}}{2\sqrt{2}} \Big| \Theta \right)$$
$$\times \ \Pr\left(\left| Im\{ \mathbf{g}^{[i]} \Theta \mathbf{h}^{[j]} \} \right| < \frac{\delta_{ji}}{2\sqrt{2}} \Big| \Theta \right) \approx \left(\frac{\delta_{ji}}{\sqrt{2\pi \nu}} \right)^2. \quad (21)$$

Proof: We defer the proof to the Appendix. ∎

Similar to Lemma 2, for any $\delta_{ji} > 0, j \neq i$

$$\Pr\left(\left| h_d^{[ji]} \right| < \frac{\delta_{ji}}{2} \Big| \Theta \right) > \Pr\left(\left| Re\{ h_d^{[ji]} \} \right| < \frac{\delta_{ji}}{2\sqrt{2}} \Big| \Theta \right)$$
$$\times \ \Pr\left(\left| Im\{ h_d^{[ji]} \} \right| < \frac{\delta_{ji}}{2\sqrt{2}} \Big| \Theta \right) \approx \left(\frac{\delta_{ji}}{\sigma_{h_d} \sqrt{2\pi}} \right)^2. \quad (22)$$

Further, for any $\Delta_{ii} > 0$, we have

$$
\begin{aligned}
\Pr\left(\left|h_d^{[ii]}\right| > \Delta_{ii}\Big|\Theta\right) &> \Pr\left(\left|Re\left\{h_d^{[ii]}\right\}\right| > \frac{\Delta_{ii}}{\sqrt{2}}\Big|\Theta\right) \\
&\times \Pr\left(\left|Im\left\{h_d^{[ii]}\right\}\right| > \frac{\Delta_{ii}}{\sqrt{2}}\Big|\Theta\right) \\
&= \left[2\int_{\frac{\Delta_{ii}}{\sqrt{2}}}^{\infty} \frac{1}{\sigma_{h_d}\sqrt{\pi}}e^{\frac{-r^2}{\sigma_{h_d}^2}}\,dr\right]^2 = \left[2Q\left(\frac{\Delta_{ii}}{\sigma_{h_d}}\right)\right]^2
\end{aligned} \quad (23)
$$

where $Q(\cdot)$ represents Q-function. Finally, we present a lower bound on the minimum number of RIS elements as follows.

Lemma 3: To achieve a per-user given value of SINR as $\widetilde{\text{SINR}}$, the minimum number of RIS elements should follow (24), shown at the bottom of the page, where $Q^{-1}(\cdot)$ is the inverse Q-function, $\log_N$ is a logarithmic function in base N, $v' = v/M$, and a shows a tradeoff between signal enhancement from the desired transmitter and suppressing the interference signals from other transmitters. For instance, we use $a = 0$ to dedicate RIS elements to reduce the interference and $a = M$ to exploit RIS elements to improve the desired signal.

Proof: Based on (6), to calculate SINR_i, we need to know the values of $|\mathbf{g}^{[i]}\Theta\mathbf{h}^{[j]} + h_d^{[ji]}|$ and $|\mathbf{g}^{[i]}\Theta\mathbf{h}^{[i]} + h_d^{[ii]}|$. Here, we aim to have $|\mathbf{g}^{[i]}\Theta\mathbf{h}^{[j]} + h_d^{[ji]}| < \delta_{ji}$ and $|\mathbf{g}^{[i]}\Theta\mathbf{h}^{[i]} + h_d^{[ii]}| > \Delta_{ii}$ at Rx_i. For simplicity, we use $\delta_{ji} = \delta$ and $\Delta_{ii} = \Delta$. Then, we have

$$
\left|\mathbf{g}^{[i]}\Theta\mathbf{h}^{[j]} + h_d^{[ji]}\right| \overset{(a)}{\leq} \left|\mathbf{g}^{[i]}\Theta\mathbf{h}^{[j]}\right| + \left|h_d^{[ji]}\right| < \delta \quad (25)
$$

where (a) follows the triangle inequality. Further, $|\mathbf{g}^{[i]}\Theta\mathbf{h}^{[i]} + h_d^{[ii]}|$ can be lower bounded by

$$
\left|\mathbf{g}^{[i]}\Theta\mathbf{h}^{[i]} + h_d^{[ii]}\right| \geq \left|h_d^{[ii]}\right| - \left|\mathbf{g}^{[i]}\Theta\mathbf{h}^{[i]}\right| > \Delta. \quad (26)
$$

The inequalities in (25) and (26) can be met if $|\mathbf{g}^{[i]}\Theta\mathbf{h}^{[j]}| < \delta/2$, $|h_d^{[ji]}| < \delta/2$, and $|h_d^{[ii]}| > \Delta + \delta/2$. We calculate the probability of these three events using (21), (22), and (23), respectively. In addition, there are N^M different RIS configurations. Thus, to have one RIS configuration that satisfies (25) and (26) from all transmitters at all receivers, we need

$$
\begin{aligned}
&N^M\left[2Q\left(\frac{\Delta + \delta/2}{\sigma_{h_d}}\right)\right]^{2K}\left(\frac{\delta}{\sqrt{2\pi M v'}}\right)^{2K}\left(\frac{\delta}{\sigma_{h_d}\sqrt{2\pi}}\right)^{2K(K-1)} \\
&> 1.
\end{aligned} \quad (27)
$$

Without loss of generality, we assume $M v' \geq \sigma_{h_d}^2$, which happens if the reflected signal through the RIS is stronger than the signal from the direct path. Then, we rewrite (27) as

$$
N^M\left[2Q\left(\frac{\Delta + \delta/2}{\sigma_{h_d}}\right)\right]^{2K}\left(\frac{\delta}{\sqrt{2\pi M v'}}\right)^{2K^2} > 1. \quad (28)
$$

To calculate (28), we assume

$$
\delta = N^{\frac{-(M-a)}{2K^2}}\sqrt{2\pi M^+ v'} \quad (29)
$$

where M^+ is the maximum value of M and $0 \leq a \leq M$ illustrates a tradeoff between improving the desired signal and suppressing the interference signals. Then, by substituting δ in (28), we obtain

$$
N^a\left[2Q\left(\frac{\Delta + \delta/2}{\sigma_{h_d}}\right)\right]^{2K}\left(\frac{M^+}{M}\right)^{K^2} > 1 \quad (30)
$$

where $(M^+/M)^{K^2} > 1$ because $M < M^+$. Thus, we need

$$
Q\left(\frac{\Delta + \delta/2}{\sigma_{h_d}}\right) = \frac{1}{2N^{a/2K}} \quad (31)
$$

to meet the inequality in (28). As a result, we calculate Δ as

$$
\begin{aligned}
\Delta &= \sigma_{h_d}\left[Q^{-1}\left(\frac{1}{2N^{a/2K}}\right)\right] - \frac{\delta}{2} \\
&\overset{(29)}{=} \sigma_{h_d}\left[Q^{-1}\left(\frac{1}{2N^{a/2K}}\right)\right] - N^{\frac{-(M-a)}{2K^2}}\sqrt{\frac{\pi}{2}M^+ v'}.
\end{aligned} \quad (32)
$$

Now, we use (6) to compute SINR at Rx_i as follows:

$$
\begin{aligned}
\text{SINR}_i &= \frac{P\left|\mathbf{g}^{[i]}\Theta\mathbf{h}^{[i]} + h_d^{[ii]}\right|^2}{\sigma^2 + P\sum_{j=1,j\neq i}^{K}\left|\mathbf{g}^{[i]}\Theta\mathbf{h}^{[j]} + h_d^{[ji]}\right|^2} \\
&\overset{(b)}{>} \frac{P\Delta^2}{\sigma^2 + P(K-1)\delta^2} \\
&= \frac{\left(\sigma_{h_d}\left[Q^{-1}\left(\frac{1}{2N^{a/2K}}\right)\right] - N^{\frac{-(M-a)}{2K^2}}\sqrt{\frac{\pi}{2}M^+ v'}\right)^2}{\frac{\sigma^2}{P} + 2\pi(K-1)N^{\frac{-(M-a)}{K^2}}\left(M^+ v'\right)} \\
&\overset{(c)}{>} \frac{\left(\sigma_{h_d}\left[Q^{-1}\left(\frac{1}{2N^{a/2K}}\right)\right] - N^{\frac{-(M^- - a)}{2K^2}}\sqrt{\frac{\pi}{2}M^+ v'}\right)^2}{\frac{\sigma^2}{P} + 2\pi(K-1)N^{\frac{-(M-a)}{K^2}}\left(M^+ v'\right)}
\end{aligned} \quad (33)
$$

where (b) holds using (25) and (26), and (c) is correct by assuming M^- as the minimum value of M. Our goal is to attain a lower bound on M that ensures $\text{SINR}_i > \widetilde{\text{SINR}}$. To do so, the right-hand side of (33) should be greater than or equal to $\widetilde{\text{SINR}}$. Consequently, we have

$$
\frac{\left(\sigma_{h_d}\left[Q^{-1}\left(\frac{1}{2N^{a/2K}}\right)\right] - N^{\frac{-(M^- - a)}{2K^2}}\sqrt{\frac{\pi}{2}M^+ v'}\right)^2}{\frac{\sigma^2}{P} + 2\pi(K-1)N^{\frac{-(M-a)}{K^2}}\left(M^+ v'\right)} \geq \widetilde{\text{SINR}}. \quad (34)
$$

$$
M \geq \min_a\left\{K^2\log_N\left[\frac{\widetilde{\text{SINR}}2\pi(K-1)\left(512v'\right)}{\left(\sigma_{h_d}\left[Q^{-1}\left(\frac{1}{2N^{a/2K}}\right)\right] - N^{\frac{-(10-a)}{2K^2}}\sqrt{\frac{\pi}{2}512v'}\right)^2 - \frac{\widetilde{\text{SINR}}\sigma^2}{P}}\right] + a\right\} \quad (24)
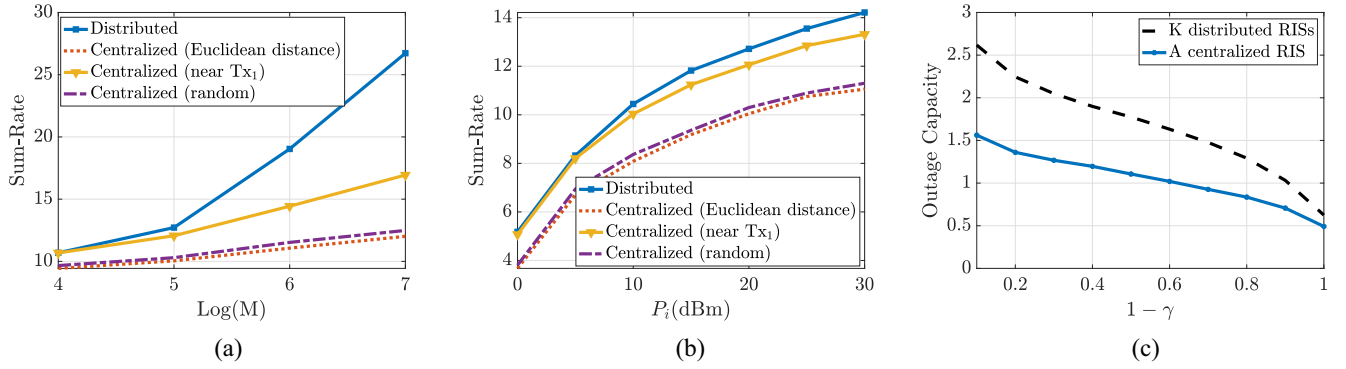$$

Fig. 2. (a) Comparison between the distributed RIS case and three different scenarios based on the centralized RIS when $K = 4$, $P_i = 20$ dB, and $M \in \{16, 32, 64, 128\}$. (b) Sum rate versus P_i using the distributed RISs and different strategies based on a centralized RIS when $K = 4$ and $M = 32$. (c) Outage capacity analysis of using a centralized RIS and K distributed RISs when $K = 4$ and the channels are noiseless.

We note that (34) depends on the value of a; therefore, by taking $\log_N$ from both sides of (34) and considering $10 < M < 512$, we derive (24), which completes the proof. ∎

Later, in Section V, we calculate the optimal value of a that maximizes the left-hand side of (34) numerically. We define $M_{\min}$ as the smallest integer that satisfies (24). Further, we refer to the curve that shows the average sum rate versus different values of P using $M_{\min}$ RIS elements as the theoretical bound.

B. Distributed RIS

In this part, we use the following lemma to show a lower bound on M that guarantees achieving a given value of $score_i$ as $s\tilde{c}ore$ in a symmetric scenario as described in Section IV-A.

Lemma 4: To achieve a per-user given value of $score_i$, as $s\tilde{c}ore$, the minimum number of RIS elements at RIS_i, where $10 < M < 512$, should follow (35), shown at the bottom of the page.

Proof: The proof is similar to Lemma 3. ∎

V. SIMULATION RESULTS

This section includes the numerical results of our proposed method. We present the results in two parts. First, we compare distributed RISs with a centralized RIS when the channels follow the small-scale fading outlined in Section II. More precisely, we study the sum rate and show the outage capacity using these two scenarios. In the second part, we assess the performance of our filled function optimization method with different benchmarks using a centralized RIS. In particular, we consider four baselines: 1) the SES method; 2) GA; 3) SR [14] method; and 4) modified SR (M-SR) [15] method. We compare our method with them in terms of rate (sum rate and minimum rate) and complexity when the channels between the APs and RIS are distributed based on the Rician fading model. Then,

we utilize a more realistic channel model where all channels follow Nakagami fading model. Finally, we study the minimum required RIS elements to provide a certain performance with a centralized RIS.

Throughout this section, we set $\sigma^2 = -80$ dBm, $\tau = 10$, $r = 10$, and $\epsilon = 0.01$, and we consider 3.5, 2, and 2.1 as the path loss exponents between the transmitters and the receivers, between the transmitters and the RIS(s), and between the RIS(s) and the receivers, respectively [39].

A. Distributed RIS Versus Centralized RIS

Sum-Rate Analysis: We investigate the performance of the distributed case with three distinct scenarios under the centralized case with noiseless channels. We regard M as the total budget of the smart surfaces, meaning that RIS_i, $i = 1, 2, \ldots, K$ contains (M/K) elements and the centralized RIS utilizes M elements. Suppose $K = 4$, $N = 4$, $C_0 = -30$ dB, the transmitters are available at $(50, 0)$, $(0, 50)$, $(100, 50)$, and $(50, 100)$, the distributed RISs are located at $(47, 4)$, $(3, 54)$, $(97, 46)$, and $(53, 96)$, and the receivers are spread at random in a room of size 100×100. We assume three scenarios for the location of the centralized RIS: 1) Euclidean distance between transmitters (i.e., $(50, 50)$); 2) near one of the transmitters [e.g., close to Tx_1 at $(47, 4)$]; and 3) at random. We consider (10) and (18) as the optimization problems with a centralized RIS and the distributed RISs, respectively. In Fig. 2(a), we show sum rate against $\log(M)$ when $P_i = 20$ dBm for $i = 1, 2, \ldots, K$. As Fig. 2(a) shows, the distributed case outperforms all scenarios with a centralized RIS and needs fewer elements to attain a given sum rate. This occurs since determining the optimal placement of the single RIS is challenging, whereas each distributed RIS is located near its associated transmitter. In addition, in Fig. 2(b), we compare the aforementioned cases

$$M > \min_a \left\{ (K-1) \log_N \left[\frac{s\tilde{c}ore \frac{\pi}{2} (K-1) \left(\sigma_{h_d}^2 + 512\nu' \right)}{\left(\sigma_{h_d}^2 + 10\nu' \right) \left[Q^{-1} \left(\frac{1}{2N^{a/2}} \right) \right]^2 - \frac{\sigma^2}{P} s\tilde{c}ore} \right] + a \right\}. \tag{35}$$
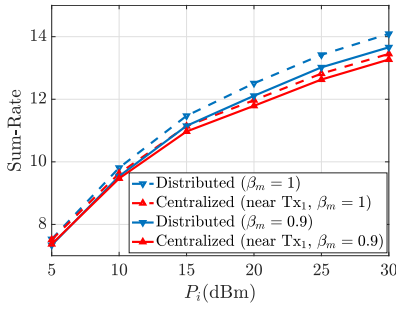
Fig. 3. Sum-rate comparison between distributed RIS and a case with a centralized RIS, where the RIS is located near Tx_1 using $\beta_m \in \{0.9, 1\}$.
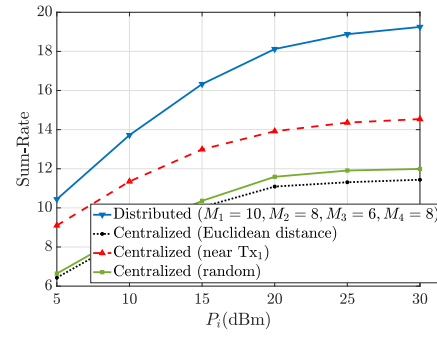

Fig. 4. Sum rate against P_i using distributed RISs, where each RIS has a different number of elements, and three cases based on centralized RIS.

when $M = 32$, $P_i \in [0, 30]$ dBm at all transmitters, and all other assumptions are the same as in Fig. 2(a). It depicts that the distributed scenario outperforms the other cases. Moreover, Fig. 2(b) shows that the curves become saturated at high-transmit power due to strong interference signals. Fig. 2(a) and (b) also illustrate that among the centralized scenarios, the case with an RIS near Tx_1 outperforms the others, while the Euclidean case performs the poorest. Here, the RIS near Tx_1 focuses on Rx_1, potentially sacrificing fairness for a higher sum rate. Conversely, the Euclidean case aims to maximize sum rate while maintaining fairness, which poses challenges. The random case falls between these scenarios, prioritizing a given user if the RIS is randomly close to the transmitter corresponding to that user and resembling the Euclidean case when RIS is positioned far from all transmitters. Thus, the random case slightly outperforms the Euclidean case, albeit remaining close to the Euclidean case, due to the lower probability of RIS proximity to any transmitter.

Outage Capacity Analysis: In this work, we mainly focus on the average rates. However, from a practical standpoint, it is important to understand the outage probability resulting in failure to achieve target rates. Thus, we study the RIS-assisted networks' outage capacity with distributed and centralized RISs under noiseless channels. We define $(1 - \gamma)$ outage capacity for the ith user, $i \in \{1, 2, \ldots, K\}$ as

$$C_i^{1-\gamma} = \{R_i : \Pr(R_i \geq R_0) \geq 1 - \gamma\} \tag{36}$$

where R_i shows the rate for the ith user in which there exists a configuration at RIS(s) with channel capacity more than or equal to R_0 with a probability greater than or equal to $1 - \gamma$. Fig. 2(c) shows the outage capacity of the centralized and distributed scenarios. In the centralized case, we assume 50, 5, and 47.17 represent the distance between Tx_i and Rx_j, $i, j \in \{1, 2, 3, 4\}$, the distance between Tx_i and the RIS, and the distance between the RIS and Rx_j, respectively. Then, in the distributed case, we consider the RISs are located at $(25, 25)$, $(25, 75)$, $(75, 75)$, and $(75, 25)$. Here, we assume other assumptions are analogous to Fig. 2(b). Fig. 2(c) shows that the distributed case provides a higher outage capacity than the centralized case, which confirms the conclusions in Fig. 2(a) and (b) that the distributed scenario outperforms the centralized scenario.

Then, we study two practical assumptions regarding RIS elements with imperfect reflection and distributed RISs with different numbers of elements in Figs. 3 and 4, respectively. Specifically, Fig. 3 assumes a case where $\beta_m = 0.9 < 1$, and the other assumptions are similar to Fig. 2(b). We compare its performance to the case with $\beta_m = 1$. Fig. 3 shows that distributed RISs provide a higher gain than centralized RIS. Further, Fig. 3 depicts a small performance degradation when we use $\beta_m = 0.9$ since the receivers get a slightly weaker signal via the transmitter-RIS-receiver link. Next, in Fig. 4, we focus on a case where each distributed RIS utilizes a different number of elements, $\mathbf{h}^{[jj]}$ is distributed based on Rician fading with κ (Rician factor) equals 2, and other assumptions are similar to Fig. 2(b). Here, Fig. 4 presents a sum-rate comparison between the distributed and centralized cases, considering a total budget of 32 RIS elements. In the distributed case, we select $M_1 = 10$, $M_2 = 8$, $M_3 = 6$, and $M_4 = 8$, where M_i, $1 \leq i \leq 4$ denotes the number of elements at RIS_i. This configuration results in a higher gain than the other cases with a centralized RIS. As observed, Figs. 3 and 4 convey a similar message to the scenario where $\beta_m = 1$ and distributed RISs have an equal number of elements. This similarity arises because the main reason for achieving better performance in the distributed scenario is that the centralized case falls short of determining the optimal RIS location, whereas each distributed RIS is positioned near its associated transmitter.

B. Efficiency of Our Optimization Method

Gong et al. [14] and Abdullah et al. [15] proposed two SR-based optimization methods, which optimize the RIS elements in an iterative fashion. In this part, we compare our filled function method with these baselines in terms of sum rate, minimum rate (min rate), and complexity. Furthermore, since the optimization problems in (10) and (11) are NP-hard problems, it is fair to utilize two other benchmarks based on heuristic optimization methods as the SES method and GA. Here, we focus on the centralized scenario and assume that $\mathbf{h}^{[ij]}$ is distributed via Rician fading with $\kappa = 2$, and the other channels follow Rayleigh fading.

Sum Rate: In Fig. 5(a), we assume $K = 4$, $N = 4$, and $P_i = 20$ dBm for $i = 1, 2, \ldots, K$. We also consider the channels are noiseless, $M \in \{8, 16, 32, 64, 96\}$, $C_0 = -30$ dB,
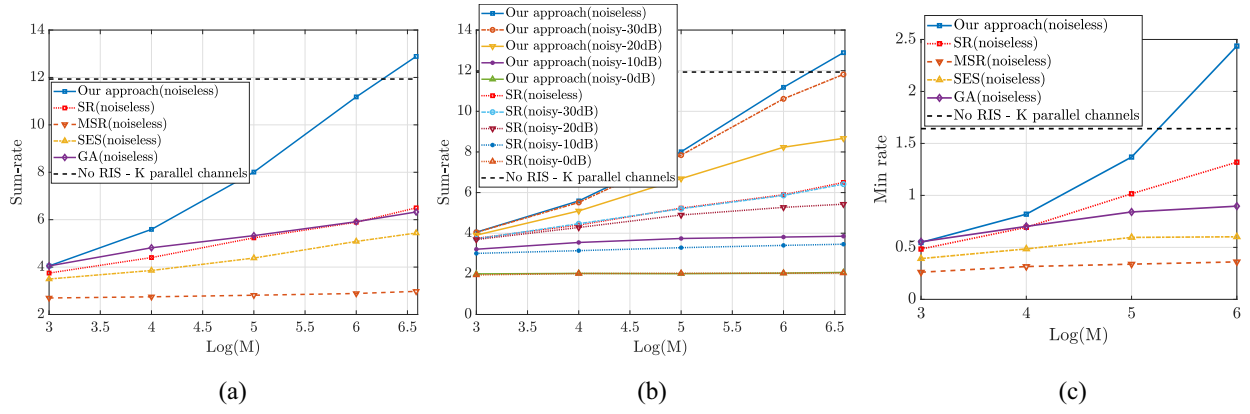
Fig. 5. (a) Sum rate against $\log(M)$ of our approach, the SR, M-SR, and SES methods, GA, and No RIS—K parallel channels under noiseless channels when $K = 4$ and $N = 4$. (b) Sum rate versus different values of M using our approach and the SR method with different versions of the noisy channels. (c) Min rate versus $\log(M)$ of our approach, the SR method, the M-SR method, the SES method, GA, and No RIS—K parallel channels under noiseless channels.

and $(0, 0)$, $(50, 0)$, and $(3, 4)$ show the locations of the APs, receivers, and RIS, respectively. Fig. 5(a) shows that our approach outperforms the SR-based methods as well as two heuristic optimization methods. Further, we consider a baseline with no RIS, referred to as "No RIS-K parallel channels," where all transmitters send their signals simultaneously and each transmitter delivers its message to its desired receiver with no interference. Fig. 5(a) shows that our method offers a higher sum rate than this baseline when $M = 96$. The gap between our approach and the benchmarks grows as M increases since our approach finds an approximate global solution by moving from one local optimum solution to another better one while the others get stuck in the local minimizers. Then, in Fig. 5(b), we present the sum rate of our approach and the SR method using both noisy and noiseless channels. It depicts that our optimization approach offers acceptable sum-rate values using noisy-30 and noisy-20 channels; however, it fails to perform well when we utilize noisy-10 and noisy-0 channels. It occurs because, as the noise power in the noisy CSI grows, the impact of using more RIS elements diminishes since the actual CSI is substantially different from the noisy CSI used in the optimization process.

Min-Rate: We focus on the max-min optimization problem in (11) to compute the min rate. The assumptions are analogous to those in Fig. 5(a). As shown in Fig. 5(c), our approach provides appreciable gains over the SR-based methods as well as GA and the SES approach due to its more efficient optimization technique. Additionally, when $M = 64$, Fig. 5(c) indicates that our approach

achieves a higher min rate than the No RIS-K parallel channels.

Complexity: In this part, we compute the complexity of our approach, the brute force search, and the baselines described in Fig. 5(a). We use the number of evaluations required to obtain the solution as a proxy for complexity, which can be derived as (37), shown at the bottom of the page, where (a) happens since $i_\ell^{\text{loc}} \leq i_{\max}^{\text{loc}}$ and $\sum_{m=0}^{(N-1)M} i_m^{\text{filled}} \leq i_{\max}^{\text{filled}}$, and (b) and (c) follow the definition of Algorithm 1 (line 7) and Algorithm 2 (line 25) where $i_{\max}^{\text{loc}}$ and $i_{\max}^{\text{filled}}$ cannot be greater than M and $N((N-1)M + 1) \lceil \log_{10}(r/\epsilon) + 1 \rceil$, respectively. In (37), we use the Landau notation ("big O") in its standard form, and $\log_{10}$ is the logarithmic function in base 10. We use the same assumptions as in Fig. 5(a) and calculate the complexity of our method, the brute force search, the SR-based methods, GA, and the SES method when $M \in \{32, 64\}$ as Table II. This table shows that our method is faster than the brute-force search and the SES method but slower than the others, revealing the rate-complexity tradeoff of the methods. Here, Table II supports the analytical complexity statement in (37).

In this work, we aim to attain the optimal RIS configuration with negligible overhead. For instance, at carrier frequency $f_c = 1.8$ GHz and at the speed of $v = 60$ km/h, the channel coherence time is equal to $c/(f_c v) = 10$ ms, where c denotes the speed of light. According to Table II, our method requires 1.45×10^6 evaluations to find the optimal solution with $M = 64$, and if we assume a dual-core processor with a clock frequency of 2 GHz, our approach requires approximately 0.36 ms to get the results, which is negligible.

$$(N-1)Mi_0^{\text{loc}} + \sum_{m=0}^{(N-1)M} \left(\frac{(N-1)Mi_\ell^{\text{loc}}}{\tau} + (N-1)Mi_\ell^{\text{loc}} \right) i_m^{\text{filled}} \overset{(a)}{\leq} (N-1)Mi_{\max}^{\text{loc}} + \frac{\tau+1}{\tau}(N-1)Mi_{\max}^{\text{loc}} i_{\max}^{\text{filled}}$$

$$\overset{(b)}{\leq} (N-1)Mi_{\max}^{\text{loc}} + \frac{\tau+1}{\tau}N(N-1)M((N-1)M+1)\lceil \log_{10}(r/\epsilon) + 1 \rceil i_{\max}^{\text{loc}} \overset{(c)}{\equiv} \mathcal{O}\left(N(N-1)^2 \log_{10}(r/\epsilon)M^3 \right) \quad (37)$$

$$d_{\mathsf{Tx}_i - \mathsf{Rx}_i} = \sqrt{d_{\mathsf{Tx}_i - \mathsf{RIS}^{[m]}}^2 + d_{\mathsf{RIS}^{[m]} - \mathsf{Rx}_i}^2 - 2d_{\mathsf{Tx}_i - \mathsf{RIS}^{[m]}} d_{\mathsf{RIS}^{[m]} - \mathsf{Rx}_i} \cos(\psi_m)} \quad (38)$$

TABLE II
COMPLEXITY OF OUR APPROACH, BRUTE FORCE SEARCH, AND THE BENCHMARKS MENTIONED IN SECTION V-B

Method	$M = 32$	$M = 64$	Method	$M = 32$	$M = 64$
Brute force	1.84×10^{19}	3.40×10^{38}	SR method	2.34×10^4	4.71×10^4
M-SR method	1.28×10^4	2.56×10^4	Genetic algorithm	2.01×10^4	2.01×10^4
Simplified exhaustive search	3.17×10^5	2.67×10^6	**Sigmoid filled function**	3.63×10^5	1.45×10^6
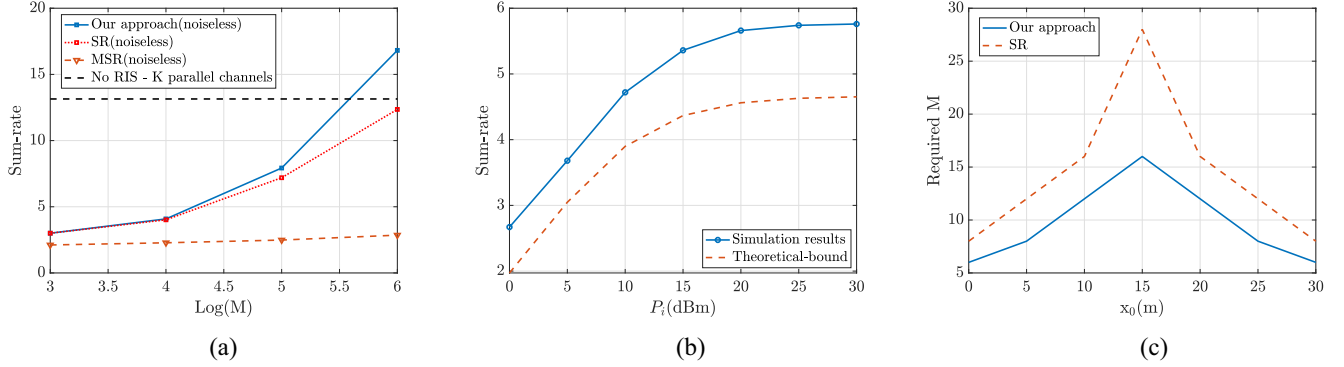
Fig. 6. (a) Comparison between our approach, the SR method, and the M-SR method using Nakagami fading when $K = 4$, and $M \in \{8, 16, 32, 64\}$. (b) Comparison between our approach and the theoretical bound with a centralized RIS when $M_{\min} = 24$, $K = 3$. (c) Number of required RIS elements to have the sum rate of 4 with one RIS when $P_i = 30$ dBm, $K = 4$, and the channels are noisy-30.

C. Nakagami Channel Model

In this part, we use a more realistic channel model based on Nakagami distribution [40]. Specifically, we define $h_m^{[j]} = |h_m^{[j]}|e^{j\bar{\theta}_{h,m}^{[j]}}$, $g_m^{[i]} = |g_m^{[i]}|e^{j\bar{\theta}_{g,m}^{[i]}}$, and $h_d^{[ji]} = |h_d^{[ji]}|e^{j\bar{\theta}_d^{[ji]}}$ as the communication channels, where $\bar{\theta}_{h,m}^{[j]}$, $\bar{\theta}_{g,m}^{[i]}$, and $\bar{\theta}_d^{[ji]}$ describe the angles of $h_m^{[j]}$, $g_m^{[i]}$, and $h_d^{[ji]}$, respectively. Here, $|h_m^{[j]}|$, $|g_m^{[i]}|$, and $|h_d^{[ji]}|$ follow a Nakagami distribution with parameters $(m_{h_m^{[j]}}, \Omega_{h_m^{[j]}})$, $(m_{h_m^{[i]}}, \Omega_{g_m^{[i]}})$, and $(m_{h_d^{[ji]}}, \Omega_{h_d^{[ji]}})$, respectively, where Ω parameters represent the large scale fading of the channels. Moreover, the angles of the channels follow independent uniform distributions. We use the cosine law to take the angle of the incident and the reflected signals at RIS into consideration. More precisely, we utilize (38), shown at the bottom of the previous page, to compute $d_{\mathsf{Tx}_i-\mathsf{Rx}_i}$, where $d_{\mathsf{Tx}_i-\mathsf{RIS}^{[m]}}$, $d_{\mathsf{RIS}^{[m]}-\mathsf{Rx}_i}$, and $d_{\mathsf{Tx}_i-\mathsf{Rx}_i}$ indicate the distance between Tx_i and the mth element of the RIS, between the mth element of the RIS and Rx_i, and between Tx_i and Rx_i, respectively. We use ψ_m to denote the angle between the $\mathsf{Tx}_i - \mathsf{RIS}^{[m]}$ and $\mathsf{RIS}^{[m]} - \mathsf{Rx}_i$ links. Fig. 6(a) depicts the comparison results between our approach and two SR-based methods using a centralized RIS when the channels are noiseless, $K = 4$, $N = 4$, and $P_i = 20$ dBm for $i = 1, 2, \ldots, K$. We assume $M \in \{8, 16, 32, 64\}$, $m_{h_d^{[ji]}} = 3$, $m_{h_m^{[j]}} = 1.5$, $m_{g_m^{[i]}} = 2.5$, $\psi_m = 86°$, $C_0 = -31.5$ dB, and $(0, 0)$, $(50, 0)$, and $(3, 4)$ are the locations of the APs, receivers, and RIS, respectively. According to Fig. 6(a), our filled function-based method provides a higher sum rate than the other baselines due to finding the approximation of the global solutions instead of the local optimal solutions.

D. Minimum Required RIS Elements

In this section, we analyze the minimum number of required RIS elements to obtain a desired performance metric. In particular, we focus on the following cases.

Theoretical Lower Bound: We assume a centralized RIS with noiseless channels and consider a symmetric setting where $K = 3$, $N = 8$, the path loss exponent between each pair of transmitter–receiver is equal to 3.9, the distance between each pair of transmitter–receiver, the distance between each transmitter and the RIS and the distance between the RIS and each receiver are equal to 25, $\sqrt{2}$, and 24.02, respectively. To obtain an accurate curve, we solve (24) numerically without utilizing the practical interval for M. In Fig. 6(b), we plot sum rate versus P_i with the theoretical bound and our approach when $M_{\min} = 24$. The results show that our method provides higher results than the theoretical bound since we obtain the theoretical-bound pessimistically (i.e., the RIS configurations are independent of the channels).

RIS at Different Locations: To study the optimal placement of the RIS, we calculate the minimum number of the RIS elements that our method and the SR method require to provide a certain sum rate when the locations of Tx_i, the RIS, and Rx_i are equal to $(0, 0)$, $(x_0, 1)$, $x_0 \in [0, 30]$, and $(30, 0)$, respectively. Moreover, we assume a symmetric setting with a centralized RIS where $P_i = 30$ dBm, the channels are noisy-30, $K = 4$, $N = 4$, and $C_0 = -30$ dB. Then, we compute the number of required RIS elements to achieve a sum rate of 4 as described in Fig. 6(c). Not surprisingly, due to the significant product-path loss, the number of required elements is highest when the RIS is placed in the middle between the transmitters and receivers, and the RIS needs fewer elements as it moves closer to either the transmitters or the receivers. Fig. 6(c) also describes that our method requires fewer elements than the SR method due to its better optimization performance.

VI. CONCLUSION

In this article, we investigated a SISO RIS-assisted IoT network under 1) centralized RIS and 2) distributed RISs,

$$\Pr\left(\left|\mathbf{g}^{[i]}\Theta\mathbf{h}^{[j]}\right| < \frac{\delta_{ji}}{2}\Big|\Theta\right) > \Pr\left(\left|Re\{\mathbf{g}^{[i]}\Theta\mathbf{h}^{[j]}\}\right| < \frac{\delta_{ji}}{2\sqrt{2}}\Big|\Theta \bigcap \left|Im\{\mathbf{g}^{[i]}\Theta\mathbf{h}^{[j]}\}\right| < \frac{\delta_{ji}}{2\sqrt{2}}\Big|\Theta\right) \tag{39}$$

with one RIS dedicated to each transmitter. The simulation results demonstrated that the distributed scenario offers a higher sum rate than the centralized case and requires fewer RIS elements to provide the same performance. We proposed an optimization approach based on a sigmoid filled function to optimize the RIS elements in the discrete domain. We showed that our optimization approach provides a higher rate and requires fewer RIS elements to meet a certain sum rate, compared to the SR-based methods [14], [15], GA, and SES methods. Finally, we evaluated the minimum required RIS elements to obtain a desired performance metric. A future direction for this work would assume a wider range for the number of distributed RISs. The main challenges are the placement of the RIS and pairing them with the transmitters.

APPENDIX
PROOF OF LEMMA 2

For a given Θ, we have a lower bound for $\Pr(|\mathbf{g}^{[i]}\Theta\mathbf{h}^{[j]}| < (\delta_{ji}/2)|\Theta)$ as (39), shown at the top of the page, where to simplify its right-hand side, we need to show that $|Re\{\mathbf{g}^{[i]}\Theta\mathbf{h}^{[j]}\}|$ and $|Im\{\mathbf{g}^{[i]}\Theta\mathbf{h}^{[j]}\}|$ are independent. Notice that the independence of the real and imaginary parts of $\mathbf{g}^{[i]}\Theta\mathbf{h}^{[j]}$ leads to the independence of $|Re\{\mathbf{g}^{[i]}\Theta\mathbf{h}^{[j]}\}|$ and $|Im\{\mathbf{g}^{[i]}\Theta\mathbf{h}^{[j]}\}|$. Based on Lemma 1, $Re\{\mathbf{g}^{[i]}\Theta\mathbf{h}^{[j]}\}$ and $Im\{\mathbf{g}^{[i]}\Theta\mathbf{h}^{[j]}\}$ are distributed via zero-mean Gaussian distribution; therefore, $Re\{\mathbf{g}^{[i]}\Theta\mathbf{h}^{[j]}\}$ and $Im\{\mathbf{g}^{[i]}\Theta\mathbf{h}^{[j]}\}$ are independent if they are uncorrelated (i.e., their covariance is equal to zero), which is straightforward. Then, for $i, j \in \{1, 2, \ldots, K\}, j \neq i$, we simplify (39) as

$$\Pr\left(\left|\mathbf{g}^{[i]}\Theta\mathbf{h}^{[j]}\right| < \frac{\delta_{ji}}{2}\Big|\Theta\right) > \Pr\left(\left|Re\{\mathbf{g}^{[i]}\Theta\mathbf{h}^{[j]}\}\right| < \frac{\delta_{ji}}{2\sqrt{2}}\Big|\Theta\right)$$
$$\times \Pr\left(\left|Im\{\mathbf{g}^{[i]}\Theta\mathbf{h}^{[j]}\}\right| < \frac{\delta_{ji}}{2\sqrt{2}}\Big|\Theta\right). \tag{40}$$

Since $Re\{\mathbf{g}^{[i]}\Theta\mathbf{h}^{[j]}\}$ is a zero-mean Gaussian random variable, for $i, j \in \{1, 2, \ldots, K\}, j \neq i$, we have

$$\Pr\left(\left|Re\{\mathbf{g}^{[i]}\Theta\mathbf{h}^{[j]}\}\right| < \frac{\delta_{ji}}{2\sqrt{2}}\Big|\Theta\right)$$
$$= \int_{-\frac{\delta_{ji}}{2\sqrt{2}}}^{\frac{\delta_{ji}}{2\sqrt{2}}} \frac{1}{\sqrt{\pi\nu}} e^{\frac{-r^2}{\nu}} dr$$
$$\overset{(a)}{\approx} \int_{-\frac{\delta_{ji}}{2\sqrt{2}}}^{\frac{\delta_{ji}}{2\sqrt{2}}} \frac{1}{\sqrt{\pi\nu}}\left[1 - \frac{r^2}{\nu} + O\left(\frac{r^4}{\nu^2}\right)\right] dr$$
$$= \frac{1}{\sqrt{\pi\nu}}\left[\frac{\delta_{ji}}{\sqrt{2}} - \frac{\delta_{ji}^3}{24\sqrt{2}\nu} + O\left(\frac{\delta_{ji}^5}{\nu^2}\right)\right] \overset{(b)}{\approx} \frac{\delta_{ji}}{\sqrt{2\pi\nu}} \quad (41)$$

where (a) applies based on approximation from the Taylor expansion of $e^{([-r^2]/\nu)}$, and (b) holds since our goal is to have a small δ_{ji}; therefore, we ignore the high orders of (δ_{ji}/ν).

Similarly, for $i, j \in \{1, 2, \ldots, K\}, j \neq i$, we obtain

$$\Pr\left(\left|Im\{\mathbf{g}^{[i]}\Theta\mathbf{h}^{[j]}\}\right| < \frac{\delta_{ji}}{2\sqrt{2}}\Big|\Theta\right) \approx \frac{\delta_{ji}}{\sqrt{2\pi\nu}}. \tag{42}$$

Hence, using (41) and (42) leads to

$$\Pr\left(\left|\mathbf{g}^{[i]}\Theta\mathbf{h}^{[j]}\right| < \frac{\delta_{ji}}{2}\Big|\Theta\right) > \left(\frac{\delta_{ji}}{\sqrt{2\pi\nu}}\right)^2 \tag{43}$$

which holds true for $i, j \in \{1, 2, \ldots, K\}, j \neq i$, and this completes the proof.

REFERENCES

[1] M. Mozaffari, W. Saad, M. Bennis, and M. Debbah, "Mobile unmanned aerial vehicles (UAVs) for energy-efficient Internet of Things communications," *IEEE Trans. Wireless Commun.*, vol. 16, no. 11, pp. 7574–7589, Nov. 2017.

[2] "Global mobile data traffic forecast update, 2017–2022," Cisco, San Jose, CA, USA, White Paper, 2019.

[3] G. Gui, M. Liu, F. Tang, N. Kato, and F. Adachi, "6G: Opening new horizons for integration of comfort, security, and intelligence," *IEEE Wireless Commun.*, vol. 27, no. 5, pp. 126–132, Oct. 2020.

[4] Z. Wang, Y. Shi, Y. Zhou, H. Zhou, and N. Zhang, "Wireless-powered over-the-air computation in intelligent reflecting surface-aided IoT networks," *IEEE Internet Things J.*, vol. 8, no. 3, pp. 1585–1598, Feb. 2021.

[5] H. Niu et al., "Joint beamforming design for secure RIS-assisted IoT networks," *IEEE Internet Things J.*, vol. 10, no. 2, pp. 1628–1641, Jan. 2023.

[6] A. Ranjha and G. Kaddoum, "URLLC facilitated by mobile UAV relay and RIS: A joint design of passive beamforming, blocklength, and UAV positioning," *IEEE Internet Things J.*, vol. 8, no. 6, pp. 4618–4627, Mar. 2021.

[7] Y. Zheng, S. Bi, Y.-J. A. Zhang, X. Lin, and H. Wang, "Joint beamforming and power control for throughput maximization in IRS-assisted MISO WPCNs," *IEEE Internet Things J.*, vol. 8, no. 10, pp. 8399–8410, May 2021.

[8] X. Li, C. Zhang, C. He, G. Chen, and J. A. Chambers, "Sum-rate maximization in IRS-assisted wireless power communication networks," *IEEE Internet Things J.*, vol. 8, no. 19, pp. 14959–14970, Oct. 2021.

[9] H. Xie, J. Xu, and Y.-F. Liu, "Max-min fairness in IRS-aided multi-cell MISO systems with joint transmit and reflective beamforming," *IEEE Trans. Wireless Commun.*, vol. 20, no. 2, pp. 1379–1393, Feb. 2021.

[10] M. Fu, Y. Zhou, and Y. Shi, "Reconfigurable intelligent surface for interference alignment in MIMO device-to-device networks," in *Proc. IEEE Int. Conf. Commun. Workshops (ICC Workshops)*, 2021, pp. 1–6.

[11] A. H. A. Bafghi, V. Jamali, M. Nasiri-Kenari, and R. Schober, "Degrees of freedom of the K-user interference channel assisted by active and passive IRSs," *IEEE Trans. Commun.*, vol. 70, no. 5, pp. 3063–3080, May 2022.

[12] Y. Ni, Y. Liu, J. Wang, Q. Wang, H. Zhao, and H. Zhu, "Performance analysis for RIS-assisted D2D communication under Nakagami-*m* fading," *IEEE Trans. Veh. Technol.*, vol. 70, no. 6, pp. 5865–5879, Jun. 2021.

[13] C. Huang, B. Sun, W. Pan, J. Cui, X. Wu, and X. Luo, "Dynamical beam manipulation based on 2-bit digitally-controlled coding metasurface," *Sci. Rep.*, vol. 7, no. 1, pp. 1–8, 2017.

[14] S. Gong, Z. Yang, C. Xing, J. An, and L. Hanzo, "Beamforming optimization for intelligent reflecting surface-aided SWIPT IoT networks relying on discrete phase shifts," *IEEE Internet Things J.*, vol. 8, no. 10, pp. 8585–8602, May 2021.

[15] Z. Abdullah, G. Chen, S. Lambotharan, and J. Chambers, "Low-complexity antenna selection and discrete phase-shifts design in IRS-assisted multiuser massive MIMO networks," *IEEE Trans. Veh. Technol.*, vol. 71, no. 4, pp. 3980–3994, Apr. 2022.

[16] B. Zheng, C. You, and R. Zhang, "Double-IRS assisted multi-user MIMO: Cooperative passive beamforming design," *IEEE Trans. Wireless Commun.*, vol. 20, no. 7, pp. 4513–4526, Jul. 2021.

[17] T. N. Do, G. Kaddoum, T. L. Nguyen, D. B. Da Costa, and Z. J. Haas, "Multi-RIS-aided wireless systems: Statistical characterization and performance analysis," *IEEE Trans. Commun.*, vol. 69, no. 12, pp. 8641–8658, Dec. 2021.

[18] S. Yang, J. Zhang, W. Xia, Y. Ren, H. Yin, and H. Zhu, "On the discrete phase shifts design for distributed RIS-aided downlink MIMO-NOMA systems," in *Proc. IEEE Wireless Commun. Netw. Conf. (WCNC)*, 2022, pp. 363–368.

[19] D. L. Galappaththige, D. Kudathanthirige, G. Amarasuriya, and C. Tellambura, "Weighted sum-rate maximization for distributed RIS-assisted cell-free massive MIMO," in *Proc. IEEE Conf. Stand. Commun. Netw. (CSCN)*, 2022, pp. 236–241.

[20] W. Mei and R. Zhang, "Multi-beam multi-hop routing for intelligent reflecting surfaces aided massive MIMO," *IEEE Trans. Wireless Commun.*, vol. 21, no. 3, pp. 1897–1912, Mar. 2022.

[21] G. Yu, X. Chen, C. Zhong, D. W. K. Ng, and Z. Zhang, "Design, analysis, and optimization of a large intelligent reflecting surface-aided B5G cellular Internet of Things," *IEEE Internet Things J.*, vol. 7, no. 9, pp. 8902–8916, Sep. 2020.

[22] Q. Wu and R. Zhang, "Towards smart and reconfigurable environment: Intelligent reflecting surface aided wireless network," *IEEE Commun. Mag.*, vol. 58, no. 1, pp. 106–112, Jan. 2020.

[23] A. Papazafeiropoulos, C. Pan, A. Elbir, V. Nguyen, P. Kourtessis, and S. Chatzinotas, "Asymptotic analysis of max-min weighted SINR for IRS-assisted MISO systems with hardware impairments," *IEEE Wireless Commun. Lett.*, vol. 12, no. 2, pp. 192–196, Feb. 2023.

[24] Q. Wu and R. Zhang, "Intelligent reflecting surface enhanced wireless network: Joint active and passive beamforming design," in *Proc. IEEE Global Commun. Conf. (GLOBECOM)*, 2018, pp. 1–6.

[25] A. Vahid, V. Aggarwal, A. S. Avestimehr, and A. Sabharwal, "On the capacity of multi-hop wireless networks with partial network knowledge," in *Proc. 48th Annu. Allerton Conf. Commun., Control, Comput. (Allerton)*, 2010, pp. 1030–1037.

[26] A. Vahid and R. Calderbank, "Impact of local delayed CSIT on the capacity region of the two-user interference channel," in *Proc. IEEE Int. Symp. Inf. Theory (ISIT)*, 2015, pp. 2421–2425.

[27] A. Vahid and R. Calderbank, "Two-user erasure interference channels with local delayed CSIT," *IEEE Trans. Inf. Theory*, vol. 62, no. 9, pp. 4910–4923, Sep. 2016.

[28] A. Vahid, V. Aggarwal, A. S. Avestimehr, and A. Sabharwal, "Interference management with mismatched partial channel state information," *EURASIP J. Wireless Commun. Netw.*, vol. 2017, no. 1, pp. 1–22, 2017.

[29] S. Nassirpour and A. Vahid, "On the stability region of intermittent interference networks," *IEEE Trans. Commun.*, vol. 69, no. 11, pp. 7335–7349, Nov. 2021.

[30] S. Nassirpour and A. Vahid, "Throughput, delay, and complexity trade-offs in interference channels," in *Proc. 10th Annu. Comput. Commun. Workshop Conf. (CCWC)*, 2020, pp. 348–354.

[31] A. Vahid, S.-C. Lin, and I.-H. Wang, "Erasure broadcast channels with intermittent feedback," *IEEE Trans. Commun.*, vol. 69, no. 11, pp. 7363–7375, Nov. 2021.

[32] S.-C. Lin, I.-H. Wang, and A. Vahid, "Capacity of broadcast packet erasure channels with single-user delayed CSI," *IEEE Trans. Inf. Theory*, vol. 67, no. 10, pp. 6283–6295, Oct. 2021.

[33] M. Grant, S. Boyd, and Y. Ye, *MATLAB Software for Disciplined Convex Programming, Version 1.21*, CVX Res, Austin, TX, USA, 2011.

[34] R. Ge, "A filled function method for finding a global minimizer of a function of several variables," *Math. Program.*, vol. 46, no. 1, pp. 191–204, 1990.

[35] C.-K. Ng, L.-S. Zhang, D. Li, and W.-W. Tian, "Discrete filled function method for discrete global optimization," *Comput. Optim. Appl.*, vol. 31, no. 1, pp. 87–115, 2005.

[36] M. Dunna, C. Zhang, D. Sievenpiper, and D. Bharadia, "ScatterMIMO: Enabling virtual MIMO with smart surfaces," in *Proc. 26th Annu. Int. Conf. Mobile Comput. Netw.*, 2020, pp. 1–14.

[37] M. Johnny and A. Vahid, "Low-complexity blind interference suppression with reconfigurable antennas," *IEEE Trans. Wireless Commun.*, vol. 21, no. 4, pp. 2757–2768, Apr. 2021.

[38] S. Nassirpour, A. Gupta, A. Vahid, and D. Bharadia, "Power-efficient analog front-end interference suppression with binary antennas," *IEEE Trans. Wireless Commun.*, vol. 22, no. 4, pp. 2592–2605, Apr. 2023.

[39] Q. Wu and R. Zhang, "Intelligent reflecting surface enhanced wireless network via joint active and passive beamforming," *IEEE Trans. Wireless Commun.*, vol. 18, no. 11, pp. 5394–5409, Nov. 2019.

[40] D. Selimis, K. P. Peppas, G. C. Alexandropoulos, and F. I. Lazarakis, "On the performance analysis of RIS-empowered communications over Nakagami-m fading," *IEEE Commun. Lett.*, vol. 25, no. 7, pp. 2191–2195, Jul. 2021.

Sajjad Nassirpour (Graduate Student Member, IEEE) received the B.Sc. degree in electrical engineering from Shiraz University, Shiraz, Iran, in 2011, and the M.Sc. degree in electrical engineering from Iran University of Science and Technology, Tehran, Iran, in 2014. He is currently pursuing the Ph.D. degree with the Department of Electrical Engineering, University of Colorado Denver, Denver, CO, USA.

His research interests include network information theory, wireless communications, machine learning, and applications of coding theory in high-performance computer memory systems.

Dr. Nassirpour has received the Best Paper Award at the IEEE Computing and Communication Workshop and Conference in 2020.

Alireza Vahid (Senior Member, IEEE) received the B.Sc. degree in electrical engineering from Sharif University of Technology, Tehran, Iran, in 2009, and the M.Sc. and Ph.D. degrees in electrical and computer engineering from Cornell University, Ithaca, NY, USA, in 2012 and 2015, respectively.

From 2015 to 2017, he worked as a Postdoctoral Research Scientist with the Information Initiative, Duke University, Durham, NC, USA, and from 2017 to 2023, he was an Assistant Professor of Electrical Engineering, University of Colorado Denver, Denver, CO, USA. He is currently a Gleason Chair Associate Professor of Electrical and Microelectronic Engineering with Rochester Institute of Technology, Rochester, NY, USA. His research interests include network information theory, wireless communications, and data storage.

Dr. Vahid received the 2015 Outstanding Ph.D. Thesis Research Award from Cornell University, the Qualcomm Innovation Fellowship in 2013, the Lab Venture Challenge Award in 2019, and the SONY Faculty Innovation Award in 2021. He currently serves as an Associate Editor for IEEE COMMUNICATIONS LETTERS.

Dinh-Thuan Do (Senior Member, IEEE) received the B.S., M.Eng., and Ph.D. degrees in communications engineering from Viet Nam National University, Ho Chi Minh City, Vietnam, in 2003, 2007, and 2013, respectively.

Before joining the University of Mount Union, Alliance, OH, USA, he was with the University of Colorado Denver, Denver, CO, USA, as a Postdoctoral Fellow in 2022. He also worked as a Research Scientist with The University of Texas at Austin, Austin, TX, USA, in 2021 and as an Assistant Professor with Asia University, Taichung, Taiwan, from 2020 to 2021. He published one textbook and five edited books. He has authored or co-authored over 100 technical papers published in peer-reviewed international journals (SCIE). His research interest includes signal processing in wireless communications network, reconfigurable intelligent surfaces, NOMA, UAV network, satellite system, physical-layer security, device-to-device transmission, and energy harvesting.

Dr. Do was a recipient of the Golden Globe Award from the Vietnam Ministry of Science and Technology in 2015 (top 10 talented young scientists nationwide). He got the Creative Young Medal in 2015. He was named to the Top List of 14 Highly Cited Scientists at Asia University in 2021. He was rewarded as the Best Editor of *ICT Express* in July 2023. He is serving as an Associate Editor in IEEE TRANSACTIONS ON VEHICULAR TECHNOLOGY and *Computer Communications*.

Dinesh Bharadia (Member, IEEE) received the bachelor's degree in electrical engineering from the Indian Institute of Technology Kanpur, Kanpur, India, in 2010, and the M.S. and Ph.D. degrees from the Electrical Engineering Department, Stanford University, Stanford, CA, USA, in 2013 and 2016, respectively.

His Ph.D. thesis invalidated a long-held assumption in wireless communication by building full-duplex radios. From 2013 to 2015, he was a Principal Scientist with Kumu Networks, Sunnyvale, CA, USA, where he worked to commercialize his research on full-duplex radios, building a product that underwent successful field trials at Tier 1 network providers worldwide like Deutsche Telekom, Bonn, Germany, and SK Telecom, Seoul, South Korea. From 2016 to 2017, he was a Postdoctoral Associate with MIT, Cambridge, MA, USA, after receiving his Ph.D. from Stanford University. From 2018 to 2022, he held an Assistant Professor position for four years with University of California at San Diego (UC San Diego), San Diego, CA, USA, and received early promotion to a Tenured Professorship. He is currently an Associate Professor with UC San Diego, the Director of the Wireless Communication Sensing and Networking Group, and part of several centers. At UC San Diego, his group WCSNG designs and prototypes systems for wireless communication, computing, sensing, networking, and sensor design with applications to privacy, security, robotics, health, and everyday life. Much of the group's research has inspired new research areas for border communities: communication theory, circuits, RFIC, and robotics. Much of his research has been translated into startups and commercial products (Haila, Kumu Networks, Totemic Labs). In the last five years, the WCSNG Research Group has received multiple awards from NSF, industry funding, and DoD funds, allowing the group to train and sustain more than 40 students at any time, training the next generation of talented engineers and scientists.

In recognition of his research, he was named a Marconi Young Scholar for Outstanding Wireless Research and awarded the Michael Dukkakis Leadership Award. He was also named as one of the top 35 innovators under 35 globally by MIT Technology Review in 2016 and worldwide by Forbes 30 under and 30 for Science category in 2018. He received the Thomas and Sarah Kailath Stanford Graduate Fellowship and a Gold Medal at the IIT Kanpur for graduating at the top of his class.